project **SPC # 004066** November 10, 2002

*FINAL REPORT*

# Phase-Equilibria and Nanostructure Formation in Charged Rigid-Rod Polymers and Carbon Nanotubes

submited to:

The European Office of Aerospace Research and Development

PI: Yachin Cohen,

Department of Chemical Engineering,

Technion-Israel Institute of Technology,

Haifa, Israel 32000.

Tel:+972 4 8292010 fax: +972 4 823076 email: yachinc@tx.technion.ac.il

# REPORT DOCUMENTATION PAGE

Form Approved OMB No. 0704-0188

Public reporting burden for this collection of information is estimated to average 1 hour per response, including the time for reviewing instructions, searching existing data sources, gathering and maintaining the data needed, and completing and reviewing the collection of information. Send comments regarding this burden estimate or any other aspect of this collection of information, including suggestions for reducing the burden, to Department of Defense, Washington Headquarters Services, Directorate for Information Operations and Reports (0704-0188), 1215 Jefferson Davis Highway, Suite 1204, Arlington, VA 22202-4302. Respondents should be aware that notwithstanding any other provision of law, no person shall be subject to any penalty for failing to comply with a collection of information if it does not display a currently valid OMB control number.

**PLEASE DO NOT RETURN YOUR FORM TO THE ABOVE ADDRESS.**

| 1. REPORT DATE *(DD-MM-YYYY)* | 2. REPORT TYPE | 3. DATES COVERED *(From – To)* |
|---|---|---|
| 18-12-2002 | Final Report | 18 September 2000 - 18-Nov-01 |

**4. TITLE AND SUBTITLE**

Phase-Equilibria and Nanostructure Formation in Charged Rigid-Rod Polymers and Carbon Nanotubes

**5a. CONTRACT NUMBER**
F61775-00-WE066

**5b. GRANT NUMBER**

**5c. PROGRAM ELEMENT NUMBER**

**6. AUTHOR(S)**

Dr. Yachin Cohen

**5d. PROJECT NUMBER**

**5d. TASK NUMBER**

**5e. WORK UNIT NUMBER**

**7. PERFORMING ORGANIZATION NAME(S) AND ADDRESS(ES)**

Technion Research & Development Foundation
Technion City
Haifa 32000
Israel

**8. PERFORMING ORGANIZATION REPORT NUMBER**

N/A

**9. SPONSORING/MONITORING AGENCY NAME(S) AND ADDRESS(ES)**

EOARD
PSC 802 BOX 14
FPO 09499-0014

**10. SPONSOR/MONITOR'S ACRONYM(S)**

**11. SPONSOR/MONITOR'S REPORT NUMBER(S)**
SPC 00-4066

**12. DISTRIBUTION/AVAILABILITY STATEMENT**

Approved for public release; distribution is unlimited.

**13. SUPPLEMENTARY NOTES**

**14. ABSTRACT**

This report results from a contract tasking Technion Research & Development Foundation as follows: The contractor will investigate 1) the mechanism of structure formation in rigid-rod and nanotube polyelectrolyte solutions using intrinsically charged rigid rods, in aqueous solutions containing acid anions and other solutes, as model systems
2) solubilization procedures for carbon nanotubes, in particular aqueous dispersion of acid-oxidized systems.
3) phase equilibria and kinetics of the solidification transition in solutions of carbon nanotubes
4) if the 10nm limit on the microfibrillar width is a fundamental limitation to rigid-rod or carbon nanotube technology or whether it can be surpassed.

**15. SUBJECT TERMS**

EOARD, Materials, Nanocrystalline Materials

| 16. SECURITY CLASSIFICATION OF: | | | 17. LIMITATION OF ABSTRACT | 18, NUMBER OF PAGES | 19a. NAME OF RESPONSIBLE PERSON |
|---|---|---|---|---|---|
| a. REPORT | b. ABSTRACT | c. THIS PAGE | | | Alexander J. Glass, Ph. D. |
| UNCLAS | UNCLAS | UNCLAS | UL | 41 | 19b. TELEPHONE NUMBER *(Include area code)* +44 (0)20 7514 4953 |

# TABLE OF CONTENTS

## Overview

The development of high performance light-weight composite materials relies on a reinforcement by rigid molecular structures. This is afforded by rigid-rod polymers, or more recently, by single-wall carbon nanotubes (SWNT). Previous experience with rigid-rod polymers has shown the limiting nanostructure to be an interconnected network of microfibrils about 10 nm in width.

The overall objective of this project is to produce processable solutions of carbon nanotubes, which can be fabricated to form desirable microstructures for high-performance applications. The nanostructures formed in solutions of rigid rod polymers and carbon nanotubes are investigated in relation to phase transformations in these systems. The underlying question is: can one control the size of the elementary microfibrils, which are formed in solutions of rigid rod polymers and carbon nanotubes, beyond the 10 nm limit?

This project is set in two parts:

Part I: The effect of coagulation conditions on the microfibril dimensions in oriented solutions of the rigid polymer poly(p-phenylene benzobisthiazole) [PBZT] in polyphosphoric acid [PPA].

Part II: Evaluation of SWNT's dispersion processes
Evaluation of amphiphilic polymers as dispersing agents for SWNTs.
Characterization of the microstructure and rheological characteristics of the SWNT dispersions:

- Inter-tube distances and overall solution microstructure in the 10-100 nm range by SAXS measurements, and various transmission electron microscopy.
- Assessment of the specific interactions in the polymer/CNT/solvent (water) system which enable dispersibility.
- Studies on spinability of the dispersions using a novel elctro-spinning apparatus to obtain oriented bundles of polymer-encapsulated CNT.

Summary of Part I

The effect of coagulation rate on the microfibril dimensions in oriented PBZT solutions was studying using the conventional rapid coagulation water as compared with slow coagulation in phosphoric acid. Slow coagulation in an acid bath was NOT able to produce significant change in the microfibril diameter. However, the microfibrils were much better aligned and the chain packing within them was enhanced.

Summary of Part II.

Stable dispersion of SWCNTs was achieved in the following amphiphilic polymers (in decreasing order of dispersing power) gum arabic, alternating copolymer of styrene and sodium maleate, polyvinyl pyrrolidone. The best dispersions were obtained with the natural polymer gum arabic. Studies on this polymer in aqueous solution indicate the origin of the dispersive interactions:

- a minority hydrophobic component can attach to the hydrophobic graphene layer.
- a highly branched, high molecular weight polymer structure with a hydrophilic nature forms a solvent-swollen protective layer due to entropic repulsion.
- charged groups at the ends of the polymer branches enhance swelling of the hydrophilic polymer layer and adds electrostatic repulsion.

Small angle neutron scattering measurements which were planned were not executed due to severe malfunction in the ISIS facility (UK).

The electrospinning process was successfully implemented using an electric field assisted take-up bobbin, by which oriented bundles of polymer-encapsulated. This was done using MWCNT dispersed in water/ethanol solutions containing poly(ethylene oxide) - PEO and surfactant (sodium dodecyl sulfate-SDS). TEM imaging displays individual tubes within PEO nanofibers, oriented along the fiber direction in some areas. Wide-angle x-ray diffraction indicated that the overall orientation achieved in the composite nanofibers was inferior to that of PEO alone. The highest orientation was achieved in PEO/SDS nanofibers, were the results indicate that both PEO crystals and SDS cylinders are oriented preferentially along the nanofiber axis.

Future work is planned using neutron scattering to quantify the structure of the polymer around the nanotube in order to better explain the dipersion mechanism. Electrospinning efforts will continue in order to enhance the overall CNT orientation. We will investigate PEO/sodium chlorate as the encapsulating medium. Such nanofibers will be studied for their electrochemical potential.

Presentations and Publications

Y. TSABBA, D.M. REIN, Y. COHEN, "Effect of Coagulation Conditions on the Microfibrillar Network of a Rigid Polymer"
Journal of Polymer Science: PartB: Polymer Physics,Vol.**40**, 1087–1094 (2002)

4th Int. Conf. on Polymer-Solvent Complexes and Intercalates, Prague (Czech Republic).Aug. 2002.
"Structure Formation during Spinning a Lyotropic Rigid-Polymer Solution *via* Different Crystal-Solvate Phases"

Polymer Fibers 2002, Manchester (UK), July 2002.
"The Effect of Coagulation Conditions on the Microfibrillar Network of a Rigid Polymer "

Rice University, Workshop on Carbon Nanotubes, Houston (August 2002)
Structural Aspects of Polymer-Nanotube Interactions

**Part I:**

The effect of coagulation conditions on the microfibril dimensions in oriented solutions of the rigid polymer poly(p-phenylene benzobisthiazole) [PBZT] in polyphosphoric acid [PPA].

A full manuscript is presented as an appendix.

ABSTRACT

An important element in the microstructure of high-performance fibers and film fabricated from rigid polymers is an interconnected network of oriented microfibrils, the lateral size of which is about 10 nm. This study is an attempt to elucidate the mechanism by which the microfibrils are formed, so that larger lateral dimensions can be achieved by suitable processing. Since this morphology emerges in the coagulation stage of the spinning process, we compared the microfibrillar network formed by drastically different coagulation conditions. Ribbons, spun from solution of poly(p-phenylene benzobisthiazole) in polyphosphoric acid through a slit die, were coagulated either in the ordinary rapid process with water (timescale of seconds) or in a slow process with phosphoric acid (timescale of hours). The coagulated microfibrillar network was dried with with supercritical $CO_2$ for x-ray scattering measurements, and impregnated with epoxy resin for sectioning and imaging by transmission electron microsocpy. Slow coagulation yields better-aligned microfibrils of enhanced chain packing, but the lateral size of the microfibrils formed in both cases is similar, about 10 nm. Heat-treatment increases the width of water-coagulated microfibrils but not the acid-coagulated ones. The observations do not support spinodal decomposition as the mechanism of microfibril formation during coagulation, as was previously suggested.

**Part II:**

Evaluation of Single-Walled Carbon Nanotube Dispersion Processes by Amphiphilic Polymers, and Processing by Electrospinning.

## Introduction

Carbon nanotubes were first discovered by Iijima[1] in 1991 revealing a new and unique structure of carbon. They are considered as elongated fullerenes built from a rolled graphene sheet forming a seamless, usually capped tubular structure. Multi-wall carbon nanotubes (MWNT) consist of several concentric layers while single-wall nanotubes (SWNT) consist just one layer forming a very thin nanotube with diameter of 0.8-1.4 nm and length of few microns. This uncommon and extremely high aspect ratio is responsible for the unique behavior, properties and applications of these quasi-one dimensional molecules.

The small dimensions and the lightweight of the carbon nanotubes combined with their exceptional properties opened a large window to a whole range of promising applications and… dreams.[2-3] Two main challenges are to be overcome in order to realize the huge potential of the carbon nanotubes: first, a large-scale production of high quality nanotubes with controlled properties is required. Secondly, these remarkable properties are attributed to the molecular level. Thus, the separation of bundles into individual nanotubes and their dispersion individually becomes vital for achieving the expected results in many applications. Among the wide range of potential applications, a few are briefly mention herein. Based on their mechanical properties, carbon nanotubes can be used as reinforcing agents of ultra strong and lightweight nano-composite materials[4] and also used to form a light and strong macro cable. Due to their size, strength, flexibility (ability to bend) and high conductivity nanotubes can be used as a nanoprobe in scanning microscope tips[5], ultrasmall pipettes for injection of molecules to cells and more. Carbon nanotubes are of best candidate to make high yeild field electron emitters due to their nano-size, high conductivity and low threshold electrical field. Field electron emitters are used for technological applications, such as flat panel displays and electron gun for electron microscopy. Recent researches use carbon nanotubes for single electron transistor (SET) which are the future alternative to conventional semiconductor transistors[6].
Also, carbon nanotubes may be used as hydrogen storage for full cells due to their high hydrogen storage capacity[7].

Preparation of stable dispersion and separation of the bundles are the crucial first steps required for any application and molecular-scale study of carbon nanotubes. Two main types of dispersions are reported in the literature: chemical and physical dispersions.

Chemical reactions of carbon nanotubes involve the attack on the carbon lattice by breaking the c-c double bond to form a covalent bond with the reactant. The oxidation of nanotubes by strong acids is one of the primary chemical reactions. Nitric acid, sulfuric acid or the combination of the two (at ratio of 3:1 $H_2SO_4$:$HNO_3$)[8-9] form acidic functional groups like carboxylic acid, carbonyl and lactone groups onto the surface of the nanotubes, leaving a hole. The acidic groups may be subsequently neutralized by base, introducing charges (like carboxylate groups), which contribute to the dispersion stability of the nanotubes in a polar solvents, especially water and ethanol, by electric repulsion. Derivatization of the acid-treated short SWNT with a long alkyl amine, as was reported by Chen at al.[10], provides the ability to solubilize the nanotubes in organic solvents, such as benzene, toluene and chloroform. Another chemical manipulation is the fluorination of SWNT[11]. In this process $F_2$ gas is reacted at high temperature with SWNT to produce side-wall fluorinated SWNT. Chemical treatment modifies the nanotubes structure and may even cause a fatal destruction of the tubes, especially SWNTs. Monthioux at al.[12] have shown that severe acid treatment in addition to the side-wall attack, causes a complete amorphisation of the graphene tubes. Morever, in contrary to other works, they proved that the chemical treatment does not exfoliate the bundles into the individual tubes. Partial recovering of the damages can be achieved by vacuum annealing at very high temperature ($1200^0$C) by regraphitization of the tube shell. However, annealed samples are more difficult to disperse, since during the annealing process larger and more well ordered bundles are formed[13]. Most of the proposed purification processes of raw materials involve an oxidation step in order to remove impurities such as catalyst particles and oxidize amorphous carbon. As the purification process is prolonged the amount of impurities decreases but the cost of damaging the nanotubes increases accordingly.

In order to disperse SWNTs the inter-tube van der Waals interaction must be overcome by other alternative physical interactions. This can be achieved by favorable adsorbing of potential candidates onto the surface of the nanotubes. In this way the dispersability is improved without damaging the nanotubes structure and their properties. One of the simplest methods is by sonicating SWNT with an ionic

surfactant, such as Sodium dodecyl sulfate (SDS)[14] or nonionic one like Triton X at a concentration below the CMC. In these systems the amphiphilic character of the surfactant stabilizes a colloidal suspension in water. However, there is no evidence that this process separates the bundles into individual tubes. In fact, viscosity measurements performed on these systems revealed a low viscosity (as water)[14], which demonstrates the colloidal/aggregated character of these suspensions.

Another approach to disperse nanotubes is based on introducing nanotubes with polymers. The similarity of the sizes and chemical structure of caebon nanotubes and certain polymers, the variety of the functional groups of the polymers and the low surface tension of liquid polymers make the polymers very good potential wetting and dispersive agents of SWNT. One of the most investigated system is a conjugated polymer Poly(*p*-phenylene vinylene) (PPV) and its derived copolymer Poly(*m*-phenylenevinylene-*co*-2,5 dioctoxy-*p*-phenylenevinylene (PmPV) solution in toluene[15-17]. The combination of the nanotubes having unique electronic properties with the conjugated polymer having optical properties opens a wide range of applications in the electro-optical field. The conjugated copolymer tends to coil forming a helical structure. Under this condition the polymer can wet the nanotubes in a close contact, which enables $\pi-\pi$ interactions to occur. Curran at al., while working with MWNT, suggested that the polymer wraps itself around nanotubes due to his helicity thus exofliating the bundles. Furthermore, it was claimed that the wrapping of the polymer (studied by transmission electron microscopy-TEM image)[18] occurs in a periodic fashion, which arises from the van der Waals interaction between the phenyl group of the polymer and the hexagonal lattice of the nanotubes. This work has been extended to SWNT[19] showing that the polymer tends to coat the nanotubes while leaving other carbon forms bare. Moreover, it was found that the polymer selectively interacts with nanotubes having specific diameters. Thus, the polymer simultaneously acts as an intercalating agent dispersing the nanotubes, purifying agent providing the separation of the nanotubes from other carboneous impurities, and selective filter of nanotubes size.

This concept of using polymer as dispersive agent was recently used by Smalley and coworkers[20] as well. In their work, SWNTs were reacted with PVP (Polyvinyl pyrrolidone) and PSS (Polystyrene sulfonate) to form a stable dispersion by replacing the self-interaction of van der Waals among the nanotubes by a strong

association between the polymer and individual SWNT. Based on atomic force microscopy (AFM) images it was once again suggested that the linear polymer is uniformly wrapped around the SWNT thus forming a uniform diameter polymer-SWNT unit. After drying, these hybrid units are easily redispersed in water by minimal sonication at concentration up to 1.4 g/l. From thermodynamic considerations it is proposed that the entropy loss due to the wrapping of the polymer around the nanotube, compared to the freely coiled conformation, is excessively compensated by the loss of the hydrophobic interaction between the nanotube surface and the surrounding water. Once the solvent is replaced by non-polar ones like THF, the thermodynamic driving force is no longer present. Thus, reversible disassociation between polymer and nanotube takes place.

A new, simple one-step process was recently reported using a natural polysaccharide, namely Gum Arabic, to disperse SWNT in aqueous solution[21]. The dispersion was prepared by simple mild sonication, resulting in a stable, visually homogeneous ink-like suspension. After drying, the nanotubes may be redispersed in water at high concentration up to 15% by weight. As was concluded from wide-angle x-ray scattering (WAXS) of the dried dispersion and reinforced by TEM images, the triangular packing of the bundles is destroyed so that individual SWNTs are well separated (the length of the separated SWNT is above 1 μm). Here, in contrast to the "wrapping" model, a more "loose" adsorbance of the polymer on the nanotubes is suggested. In this configuration the polymer chains are adsorbed to the nanotubes without loosing their coiled conformation. The repulsive entropy between the polymer chains, which are immersed in a good solvent having en excluded volume, overcomes the van der Waals attraction between the embedded nanotubes. On the other hand, the exfoliation of the bundles into individual tubes is accompanied by an increase of the overall translational entropy since the number of the separated units is larger relative to the bundled state. Both contributions encourage the separation of the nanotubes and stabilize the dispersion.

So far, only few reports have been presented concerning the processing of carbon nanotube dispersions to a final macroscopic product. One of the first attempts was done by Vigolo and co workers[14]. This work introduced a way to assemble SWNTs into a macroscopic long ribbon or fiber. The SWNTs (0.4 wt%) were dispersed by sonication in an aqueous solution of the anionic surfactant SDS (1 wt%).

At intermediate concentration of SDS, a stable homogeneous dispersion was formed due to electrostatic repulsion between the adsorbed surfactant molecules. The viscosity of this dispersion was "as low as water". This dispersion was injected through a syringe needle into a rotating solution of polyvinylalcohol (PVA). PVA adsorbed onto the nanotubes due to its amphiphilic character replacing some SDS molecules but in the lack of electrostatic repulsion immediate aggregation took place. Both shearing flow at the tip of the needle due to the relative high viscosity of the PVA solution, and elongation flow achieved by the rotating flow drawing the dispersion filament in a spiral path, induced the alignment of the nanotubes bundles and formation of a ribbon. By pumping the PVA solution from the bottom, a long ribbon without entanglements could be drawn out easily. The Young's modulus of these fibers after rinsing and drying varied between 9-15 GPa which is much lower then the individual nanotubes but is one order of magnitude greater than the modulus of the "bucky paper". X-ray diffraction of these fibers[22] has shown that the nanotubes as well as PVA and residual graphite preferentially oriented along the fiber axis. Yet, the distribution of nanotubes orientation is still large as indicated by FWHM ($75^0$) of the angular distribution peak. Another method to process nanotubes dispersion was applied by Schreuder-Gibson at al.[23] using the electrospinning technique. In this work carbon naotubes were dispersed in a solution of polyurethane in DMF (dimethylformamide) and polyaniline to produce a spinnable solution (10% polymer, 10% carbon nanotubes and 80% DMF). The solution was electrospun, resulting in a composite nanofiber enclosing oriented clusters of nanotubes along its axis (see section 2.2.5.2). A new work just published[24] demonstrated the formation of a hybrid fiber by dry jet wet spinning technique. In this case a liquid crystalline phase of poly(para phenylene benzobisoxazole) (PBO) was prepared by *in situ* polymerization of the monomers in the present of SWNTs (~10 wt% of the polymer weight). The resulting hybrid fiber exhibited tensile strength greater by a factor of 50 than the PBO fiber.

## Research Objectives

Realization of the superior molecular properties of single-wall carbon nanotubes (SWNTs) in a large-scale product is strongly bound to the "quality" of the nanotubes dispersions and their processability. To date, the properties of the macroscopic products (mechanical properties in particular) are far below the molecular properties. Hence, progress on practical applications has been held back.

The control over the dispersion preparation, the characterization in both nanometric and macroscopic scale and the understanding of the driving forces stabilizing these dispersions are the primary aims of this work. Based on achieving these aims, an attempt to produce macroscopic oriented fibers and nanofibers representing a scaled-up unit of the SWNT and its unique mechanical properties, will be done.

In order to gain the overall aim the following objectives are presented. The objectives begin with nano-scale analysis and lead up to production and characterization at macroscopic level:

(1) Establishing a well defined controllable procedure for dispersing SWNT in aqueous polymer solutions.
(2) Nanoscale characterization of the resulting dispersions in terms of structures and sizes dominating the dispersions. This will provide an answer to the fundamental question as to whether the dispersion is a molecular dispersion resulting from a total disassociation of the SWNT bundles or rather an aggregated dispersion.
(3) In even deeper detail – defining the nature of the interactions between the polymers and the SWNTs which are responsible for the stabilization of the dispersion: Where is the polymer located? How does it associate with the nanotubes? The answers to these questions will lead to better understanding of the forces playing a role in these systems and the thermodynamic motivation for stability.
(4) Processing the SWNT dispersion into a macroscopic structure: A well aligned macroscopic fiber will be produced by spinning and electrospinning, and a "composite" nanofiber containing polymer and SWNT will be produced by electrospinning.

## Materials and Methods

(a) Single-wall carbon nanotubes (SWNT)

SWNTs were purchased from Carbon Nanotechnology Inc. These SWNTs are produced by the HiPco method. The average diameter of HiPco SWNTs is approximately 1.1 nm[25]. The dominant impurity residue from this production is iron catalyst, which form small particles at size of 3-5 nm and are enclosed in thin carbon shells. Another characteristic of this material is its extremely low bulk density on the order of 0.01 g/cc. Hence, this lightweight material is very difficult to handle and to prepare solution with since it floats above almost any liquid. Vigorous shaking is required for the initial dispersion in order to bring into contact the liquid and the SWNTs.

The raw SWNTs were also purified by a specific procedure, which has been developed for HiPco SWNTs specifically[25]. This procedure is based on gas-phase oxidation and extraction of the catalyst.

For comparison a small quantity of SWNTs from Carbolux Inc. were obtained- As Produced (AP) grade.

(b) Polymers

In this work, several polymers were investigated as dispersive agents for SWNTs.

Gum Arabic

This natural is prepared from the stems and branches of sub-Saharan *Acacia senegal* and *Acacia seyal* trees. It is a complex and variable mixture of arabinogalactan oligosaccharides, polysaccharides and glycoproteins, ansd is used in food technology as an "excellent emulsifier with very low viscosity". Its major component is a highly branched polysaccharide (M.Wt. ~$0.25 \times 10^6$), the side branches of which end in charged glucoronic acid . The minor component is a higher molecular weight hydroxyproline-rich glycoprotein (M.Wt. ~$2.5 \times 10^6$). The total (hydrophobic) protein content is ~ 2%

Alternating styrene/maleic anhydride copolymer

Alternating amphiphilic copolymer may represent the wrapping model suggested by Smalley and co-workers where the short styrene units lay on the nanotubes and the short neutralized maleic units oriente toward the water. The

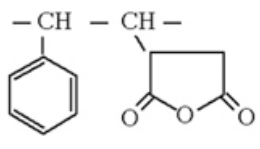

copolymer was purchased from Sigma-Aldrich. Styrene and Melaic anhydride tend to form almost full alternating copolymer composition, usually by radical polymerization. The maleic anhydride group were neutralized to form carboxylate groups. The neutralization will be done by boiling the copolymers in NaOH solution for 2 hours. The degree of neutralization is controlled by the number of NaOH moles. The charged carboxylate groups will stabilize the dispersion by electrostatic repulsive interaction.

PVP- Poly vinyl pyrrolidone

This homopolymer is also amphiphilic and has been already used to disperse SWNT as was reported by O'Connell et al. [20]

(c) Transmission electron microscopy (TEM)

Transmission electron microscopy (TEM) observation was performed with a Philips CM120 transmission electron microscope. In particular, the technique of Cryo-TEM for direct observation of vitrified thin films of aqueous dispersions was done as described in detail elsewhere[26]. In brief, a 3 mL drop of aqueous dispersion is placed on a perforated carbon-film-coated TEM copper grid and excess liquid is blotted with filter paper to produce a thin (about 300 nm) liquid film supported on holes (several micrometers in diameter) in the carbon film. The grid is then plunged into liquid ethane at its freezing point and vitrified. We performed specimen preparation in the Controlled Environment Vitrification System (CEVS) at 25 $^{o}$C and 100% relative humidity. The vitrified specimens were stored under liquid nitrogen and transferred to an Oxford CT3500 cooling-holder of the Philips CM120 TEM, where they were examined at a temperature of about -180 $^{o}$C. Low electron dose imaging (less than 20 electrons per Å$^2$) was carried out using an acceleration voltage of 120 kV. Images were recorded with a Gatan MultiScan 791 CCD camera, using the Gatan DigitalMicrograph 3.1 software package.

(d) Small-angle x-ray scattering (SAXS)

SAXS measurements were performed using a slit-collimated Kratky compact camera (A. Paar Co.), with Ni filtered Cu$K_\alpha$ radiation from a sealed tube generator (Philips PW1730) at 40kV and 30mA. Dispersions were placed in thin-walled glass capillaries (1 mm diameter, 0.01 mm wall- thickness). The sample to detector distance

was 260mm. In data analysis the intensity is portrayed as a function of the scattering vector $h$ which is defined as: $h = 4\pi \sin\theta / \lambda$ where $2\theta$ is the scattering angle and $\lambda$ is the wavelength. The scattered intensity was measured with a linear position-sensitive detector (Raytech) coupled to a multichannel analyzer (Nucleus III). The increment of scattering vector per channel was $0.0126 nm^{-1}$. Absolute intensity units were determined with a secondary standard (thin glass slide) pre-calibrated with a moving slit device.

## Results

### Dispersions

Dispersions were prepared using published methods and materials as well as new potential dispersive polymers. All polymers used have an amphihpilic character, which may provide the stabilization of aqueous dispersion of the hydrophobic carbon nanotubes.

SWNTs purchased from CNI (HiPco process) were mainly used in these experiments. TEM and SEM images of the raw material are presented in **Figure 1**. The raw material was sonicated in methanol and a drop of this dilute dispersion was dried on a polyimide-coated copper grid for TEM imaging. As can be clearly seen, the material contains many catalyst particles at a size of 2-3 nm. In addition, the SWNTs are arranged in bundles consisting of several nanotubes each, as expected. In the SEM image, a typical dense network of entangled SWNTs is observed.

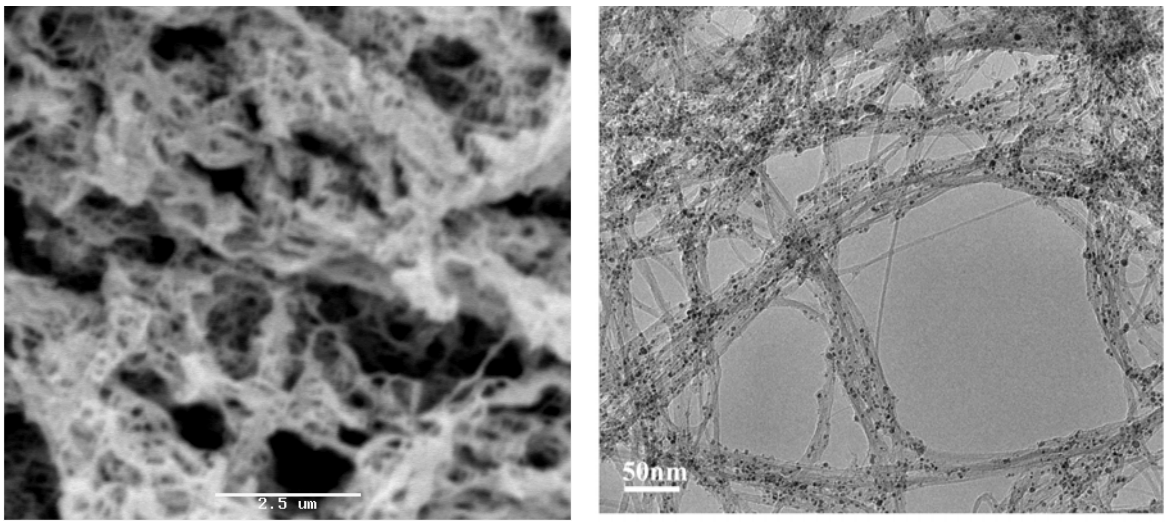


Figure 1: SEM(a) and TEM (b) images of HiPco carbon nanotubes raw material.

After a purification procedure developed by Chiang et al.[25], the majority of catalyst particles have been removed as shown in **figure 2**.

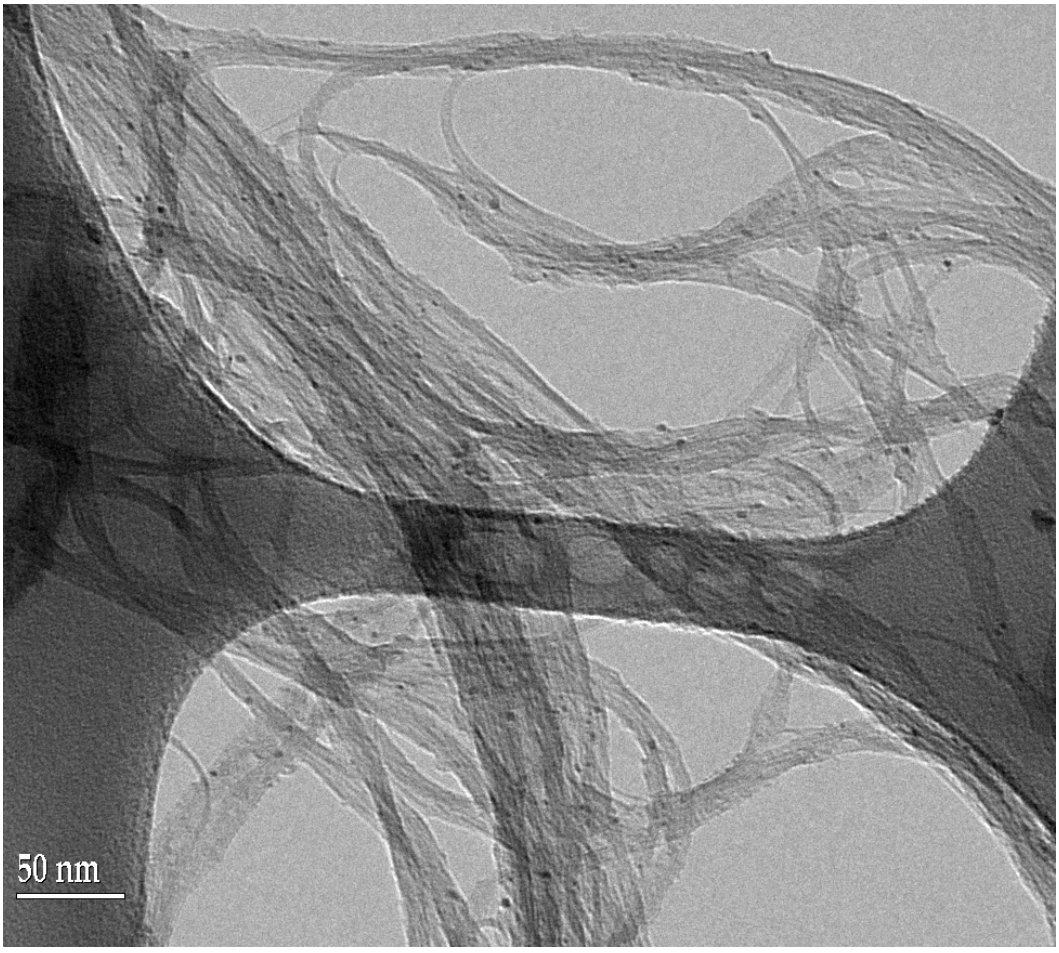


Figure: 2 TEM micrograph of purified HiPco SWNT

The following table summarizes the different dispersions that have been prepared:

| Dispersion | Composition | Procedure | Appearance |
|---|---|---|---|
| HiPco SWNT+ SDS | 1 % wt SDS<br>0.35% wt SWNT | 3 hrs sonication | Unstable dispersion. Aggregated dispersion |
| HiPco SWNT+ GA | 1%, 5 % wt GA<br>0. 5% wt SWNT | Preparation of the GA solution first and than 2 hrs. sonication | A homogenous stable solution was achieved only after wetting problem has been overcome by first wetting the nanotubes with methanol and evaporating. |
| MWNT+GA | 1% GA<br>0.35 % MWNT | ½ hr. sonication. Easy handling and wetting properties | A homogenous stable ink-like solution. |
| HiPco SWNT + PS16 | ~1.8% wt PS16<br>0.5 % SWNT | 9 hrs. sonication | Phase separation |
| HiPco SWNT + PS10L * | ~1.4% wt PS10L<br>0.5 % SWNT | ½-1 hr sonication | A homogenous stable ink-like solution but still contain very fine powder-like aggregates |
| HiPco SWNT + PSSty * | ~1% wt PSSty<br>0.5 % SWNT | ½-1 hr sonication | A homogenous stable ink-like solution |

* No prewetting of the nanotubes with methanol was required in the preparation of the dispersion with PS10L and PSSty.

**Gum Arabic (GA) dispersions**

In order to reveal the structural association between the carbon nanotubes and the GA, small- angles x-rays scattering was used.

The scattering curves of both dispersion of SWNT with GA and GA solution in the same concentration are presented in figure **3**. It is clearly seen that the contact between carbon nanotubes and GA introduces structural changes of the GA. The peak observed in the GA solution disappears in the dispersion.

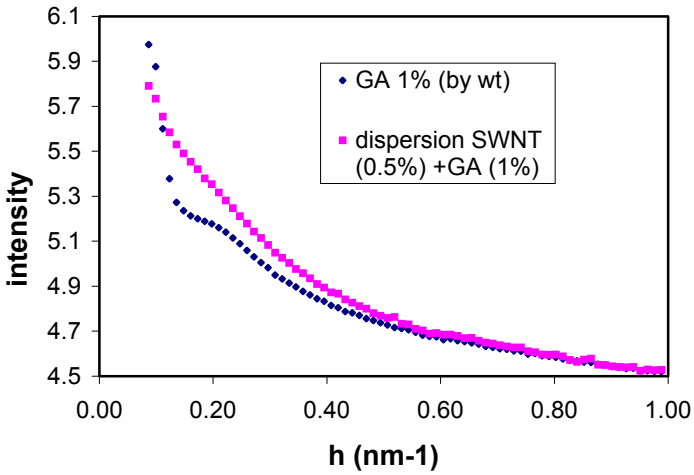


Figure 3: SAXS curves of carbon nanotubes' dispersion with GA and GA solution.

This observation was further investigated by measuring the scattering pattern of GA alone at different concentrations as presented in **figure 4**. Indeed, the unknown peak of GA is repeated in all concentrations. However, both the location and the shape of the peak are concentration depended. As the concentration increases the peak shifts to larger scattering vector and becomes broader. This behavior points out to the fact that these peaks are related to the structure factor i.e. the inter-distances between "paricles" of GA- the so called inter-micillar peak. At 30% the peak becomes significantly broader due to the dense of the particles, which already start to overlap. Viscosity measurements performed by Yerushalmi-Rozen and co workers[21] showed that the c* (overlapping concentration) at which the viscosity starts increasing sharply is around 30%. This result is in a good agreement with the scattering results.

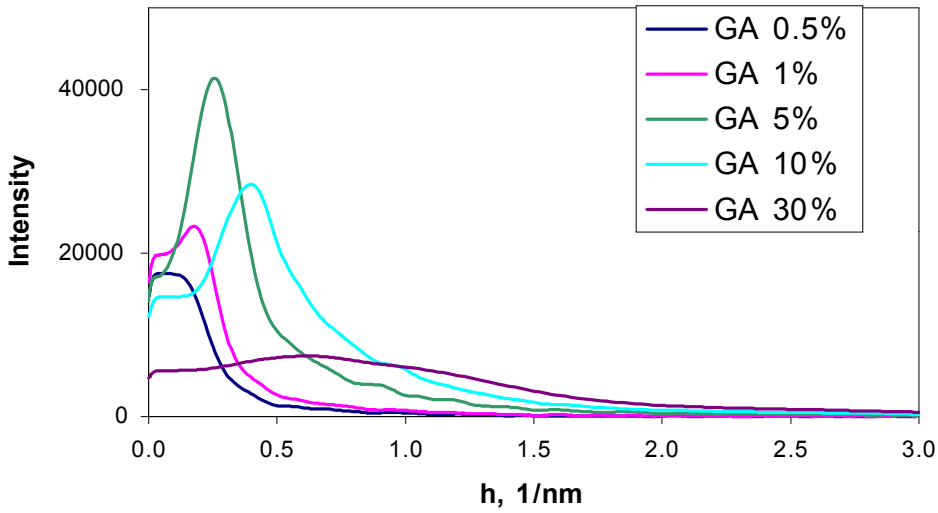


Figure 4: SAXS curves of GA solutions at different concentrations.

The d-spacing, determined from the peak position (*h**) and Bragg's law ($d = \frac{2\pi}{h^*}$), is shown as function of concentration ($c$) in **figure 5**. A power law $d \sim c^{-1/3}$ describes this dependence. The –1/3 power law is typical to the arrangement of globular particles on a three-dimensional lattice. Moreover, the "ordered" inter-aggregates distances may indicate a stabilizing electrostatic force.

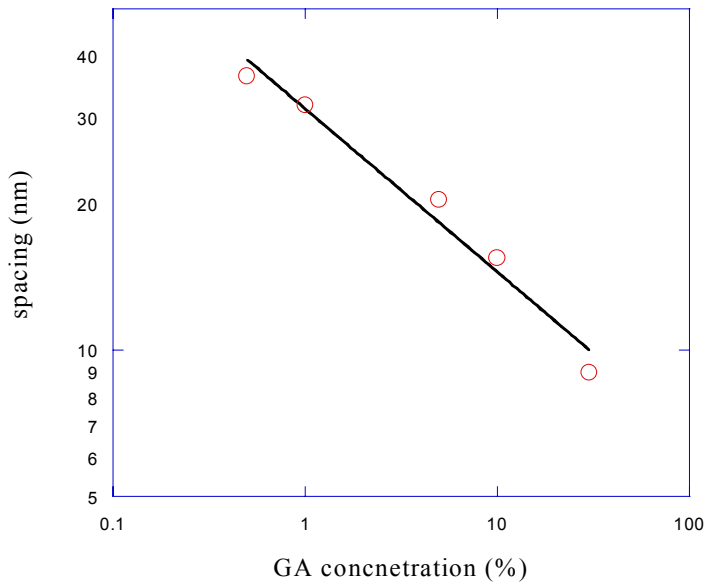


Figure 5: d-spacing versus concentration of GA

Since GA is a complex multi-component material, we tried to evaluate the contribution of its main components in order to gain further understanding of the GA structure.

The scattering curves of Arabinogalactan, which is the main branched polysaccharide component of GA at the same concentrations as GA are presented in **figure 6.** A pronounced difference between GA and its polysaccaride is observed, as can be seen more clearly in **figure 7**. The scattering curve of arabinogalactan in the absence of the hydrophobic glycoprotein, is typical to a semi-dilute polymer solution and no peak is observed.

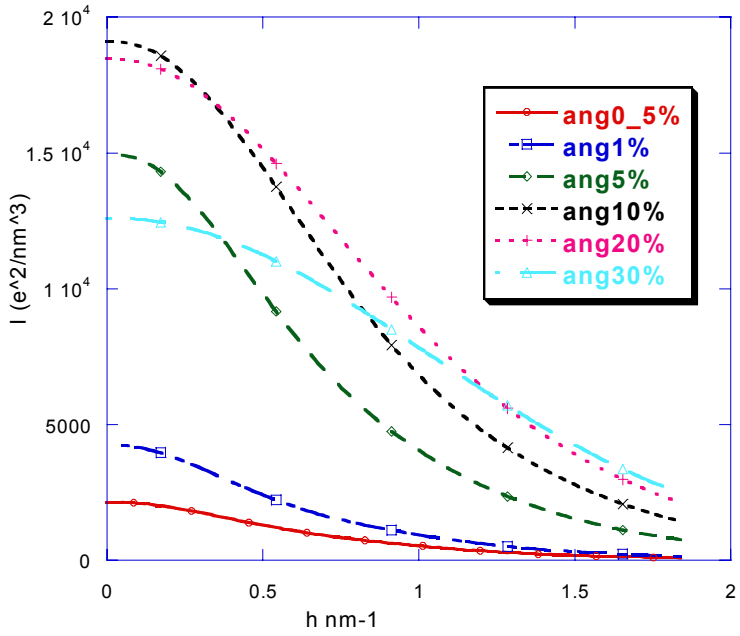


Figure 6: SAXS curves of Arabinogalactan at different compositions.

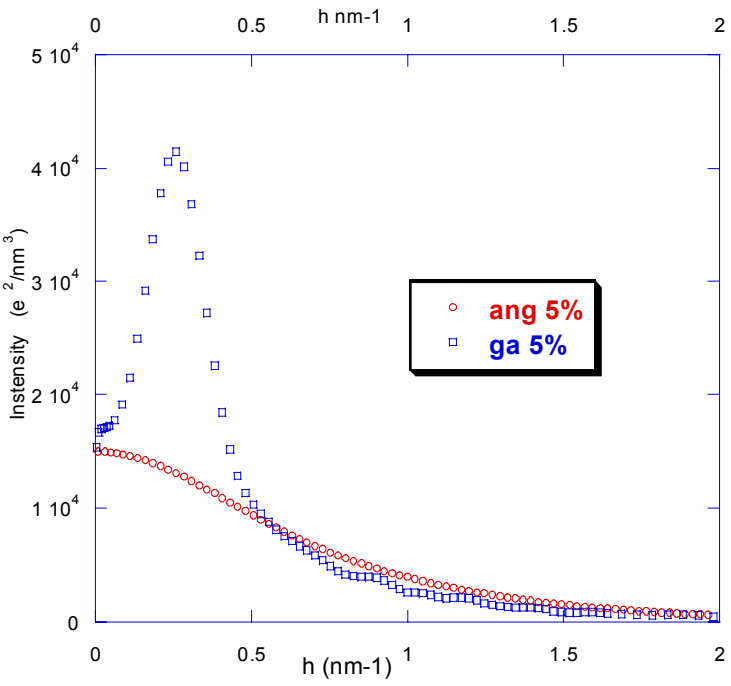


Figure 7: Comparison of the SAXS curves of GA and Arabinogactan at 5% concentartion.

Based on these results it may be suggested that the GA in water is arranged in a kind of "unordered" micelle or kind of a dendrimer where the hydrophobic glycoprotein is compact into a small core while the hydrophilic charged polysaccharide form a branched large "shell" as illustrated in the **figure 8**. A TEM micrograph of 5 % wt GA is given in **figure 9**.

As the carbon nanotubes are introduced to this "surfactant" system, the dendrimer structure is destroyed, as was seen in figure no. 3, and the hydrophobic glycoprotein is adsorbed at the hydrophobic surface of the carbon nanotubes. The charged polysaccharide in turn is responsible for the steric and charge stabilization of the dispersion thus separates the bundles to smaller bundles and even individual nanotubes.

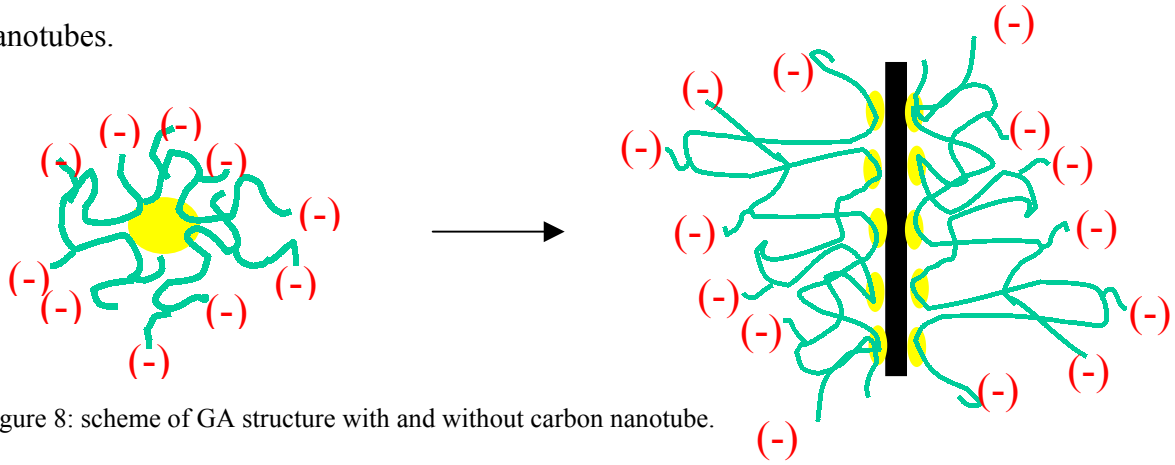


Figure 8: scheme of GA structure with and without carbon nanotube.

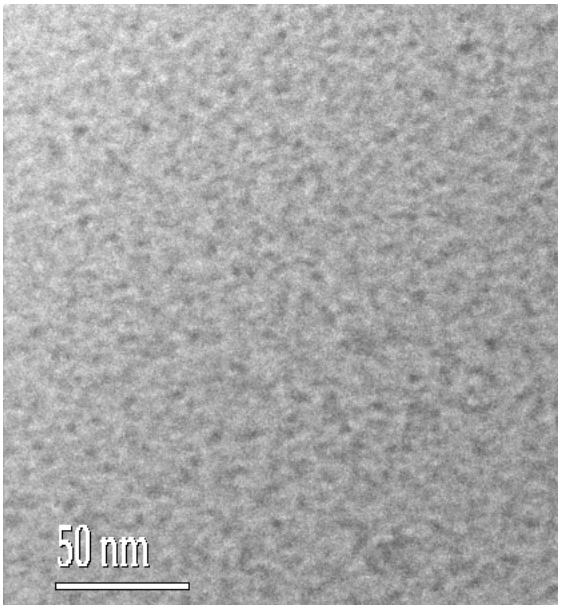


Figure 9: TEM micrograph of 5 % wt GA.

**“Polysoap” dispersions**

Alternating copolymers of ionized maleic acid with hydrophobic monomers were used to disperse carbon nanotubes. As summarized in **table 1**, PSSty and PS10L enabled formation of a stable ink-like dispersion while PS16 has failed. The scattering curves of both the dispersions and the copolymer solutions without nanotubes are presented in **figure 10**. As with GA, the addition of the carbon nanotubes to the copolymer solutions induces significant structural changes especially in PS10L and PSSty solutions. The micellar peaks of PS10L and PS16 are clearly observed however the peak of PS10l totally disappears in the dispersion with nanotubes while the one of PS16 still appears although slightly masked by the scattering of the nanotubes. This different indicates the difference in the “quality” of the interaction between the two copolymers and carbon nanotubes. PSSty doesn’t form micelles. Nevertheless, the scattering curve is significantly altered showing a specific interaction between the copolymer and the carbon nanotubes.

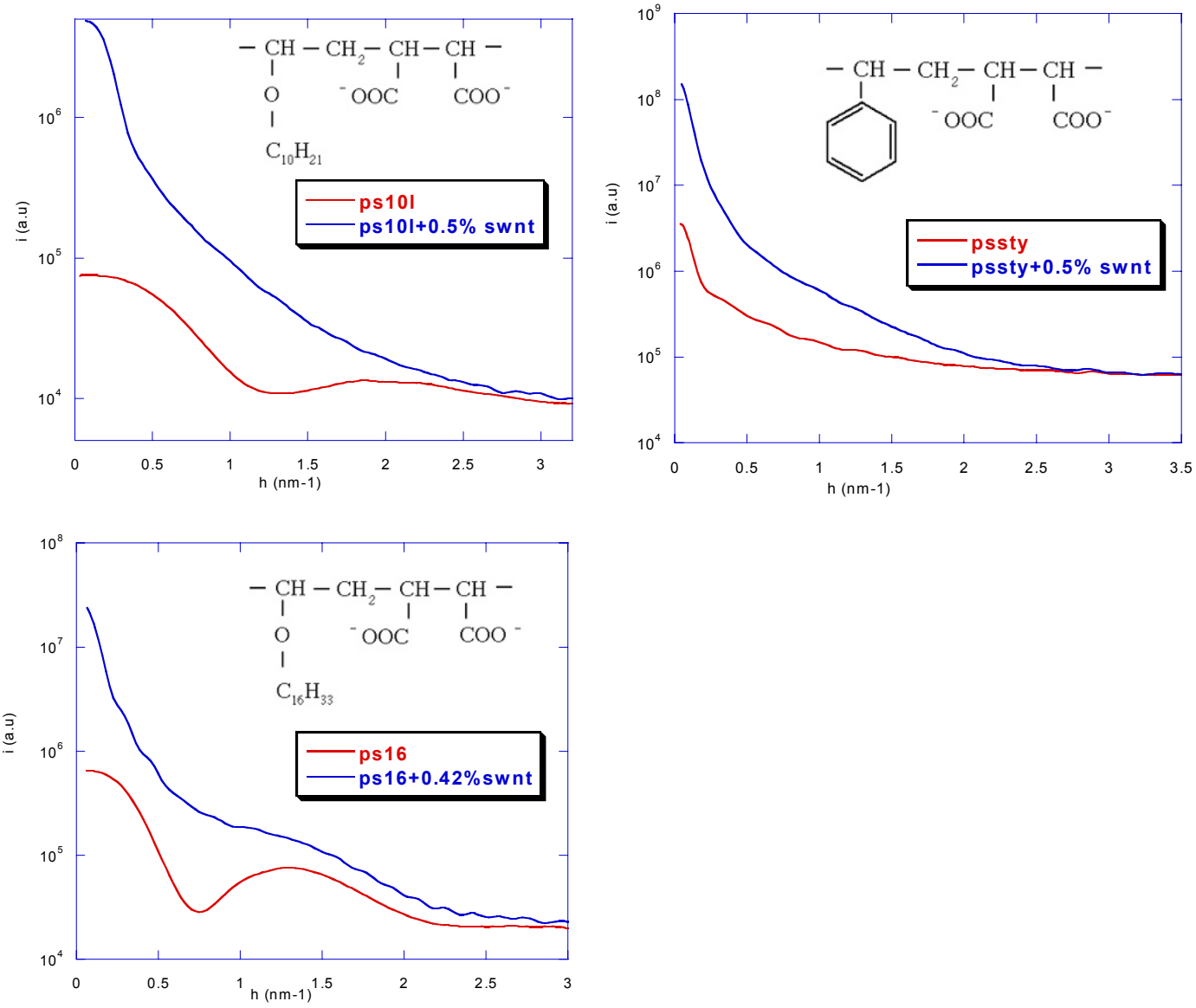


Figure 10: SAXS curves of carbon nanotubes dispersions with "polysoaps" and "polysoaps" solutions.

Log-log presentation of the desmeared (after correction of the slit length of the incident beam) scattering curves of the dispersions is shown in **figure 11**. The results show that the final slop of the scattering curves follows Porod 's $h^{-4}$ power law of a particulate system, in accord with the findings of Rols et al.[27]

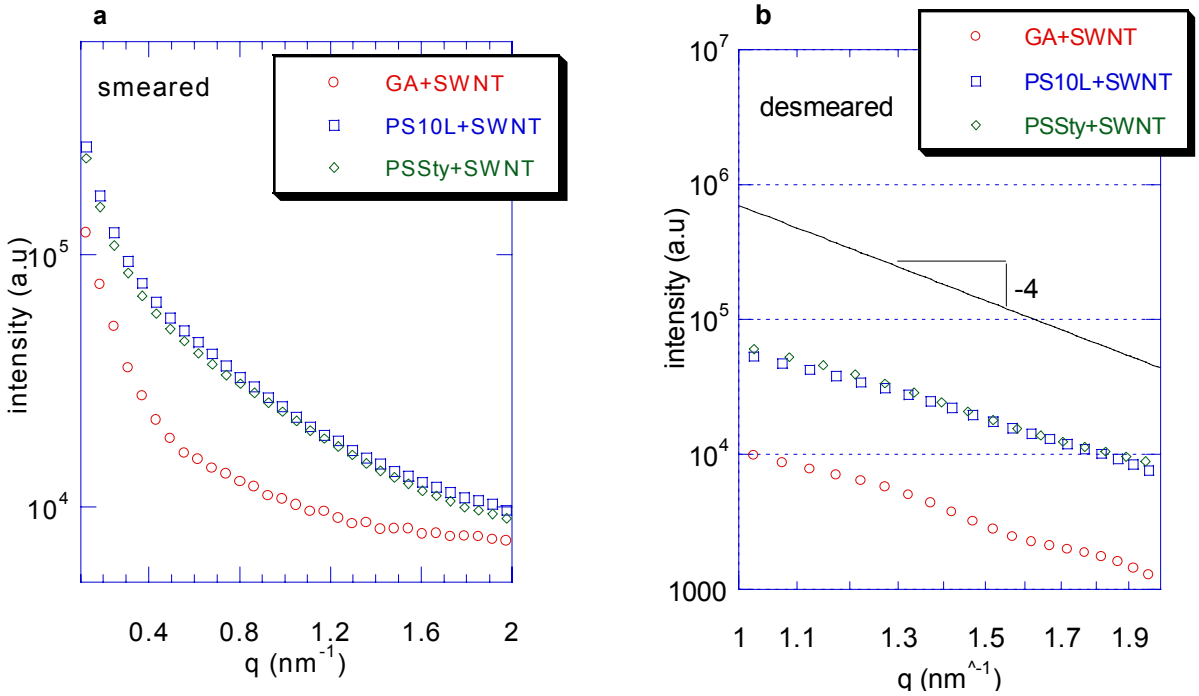


Figure 11: SAXS curves of dispersions of SWNT + polymers. (a) silt smeared data
(b) final slop of the scattering curve for desmeared data.

The characteristic size of the particles can be evaluated using the Guinier approximation for the cross section of the form factor at very small angles and Porod's law of the final slope for a two-phase system with sharp boundaries:

Giunier approximation $i(q)q = i(0)\exp(-r_c^2 q^2/2)$ for $q<1/r_c$

Porod's law $\lim_{q\to\infty} i(q) = 2\pi(\Delta\rho)^2 S/V \cdot \frac{1}{h^4} = \frac{4Q}{\xi}\cdot\frac{1}{h^4}$ for $q>1/\xi$

Were, $r_c$ is the mean radius of gyration of the cross section of a rod-like particle and $\xi$ is the characteristic length and Q is the integrated intensity, termed the invariant. Q is defined by $Q = \int_0^\infty i(q)q^2 dq$

These characteristic lengths are given in **Table 2**. These results may suggest partial separation of the bundles in the dispersions.

| | $r_c$ (nm) | $\xi$ (nm) |
|---|---|---|
| GA+0.5% (w) SWNTs | 3.0 | 3.5 |
| PS10L+0.5% (w) SWNTs | 2.0 | 2.1 |
| PSSty+0.5% (w) SWNTs | 2.1 | 2.4 |

Table 2: calculated characteristic lengths.

In addition a clear difference between the scattering curve of the GA dispersion and the copolymers dispersions is observed. This difference is to be further investigated in order to reveal the character of the dispersions.

A TEM micrograph (**figure 12**) of the dispersion of unpurified HiPco SWNT with PSSty shows that the dispersion contains very small bundles which seem as individual nanotubes and larger bundles consist of few nanotubes but much less than in the raw material. Also, it is lucid that the individual nanotubes contain no catalyst particles while the larger bundles contain a lot of catalyst particles. This fact may serve as a mark for individual nanotubes.

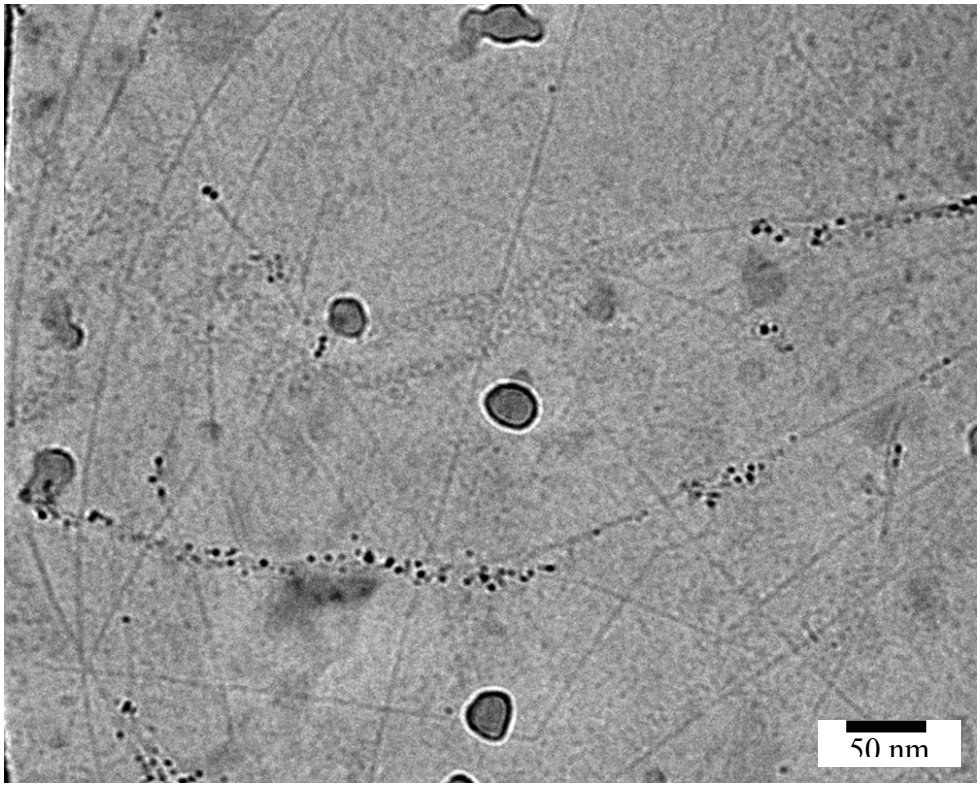


Figure 12: TEM micrograph of HiPco SWNT dispersion with PSSty.

**SDS and poly(vinyl pyrrolidone) dispersion**

Dispersion of HiPco SWNT in water with sodium dodecyl sulfate [SDS] and poly(vinyl pyrrolidone) [PVP] was prepared and sent to us by Dr. Strano of Professor Smalley's group in Rice University. It was prepared according to the process reported by O'Conell et al.[20].

X-ray scattering curves of the dispersion and the mixture of SDS and PVP are given in **figure 13**. The finger-prints of SDS are clearly seen by the inter-micellar peak (~ 0.5 $nm^{-1}$) and the micellar peak at 1.5 $nm^{-1}$. The inter-micellar peak is overshadowed in the dispersion curve due to the scattering of the nanotubes. The micellar peak though, is broader and may consists of 2 peaks as can be seen in a close view (**figure 13 c**). It may be suggested that the first peak (at 1.5 $nm^{-1}$) is assigned to the original 5 nm diameter SDS micelle while the second shifted to smaller angle (at 1.3 $nm^{-1}$), is attributed to larger micelles of about 5.8 nanometer built from SDS molecules around single carbon nanotubes. Further investigation is required to confirm this suggestion.

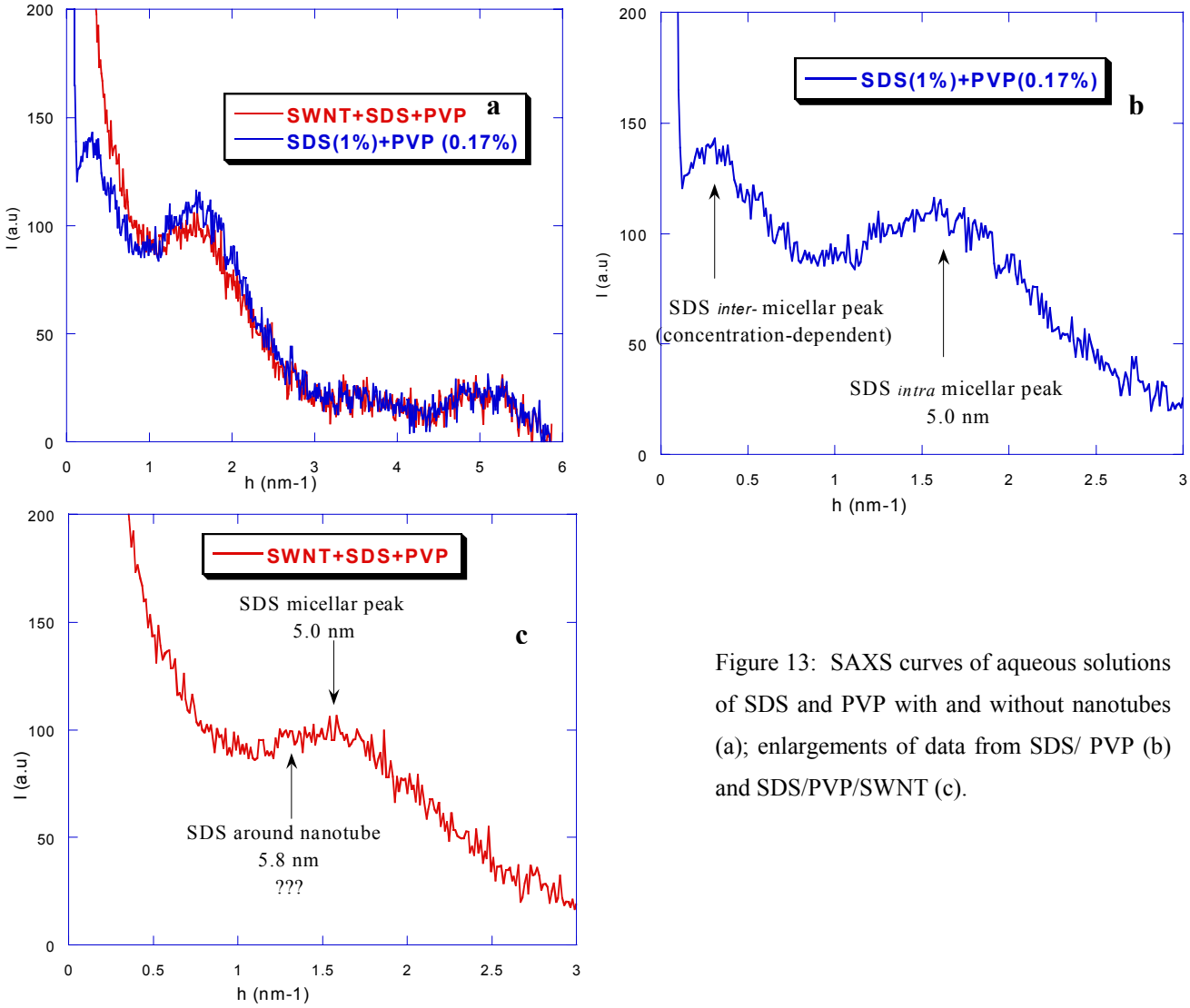


Figure 13: SAXS curves of aqueous solutions of SDS and PVP with and without nanotubes (a); enlargements of data from SDS/ PVP (b) and SDS/PVP/SWNT (c).

Cryo-TEM micrographs of this system are shown in **figure 14.** Individual carbon nanotubes as well few smaller bundles can be observed in addition to micelles of excess SDS (**figure 14b)**.

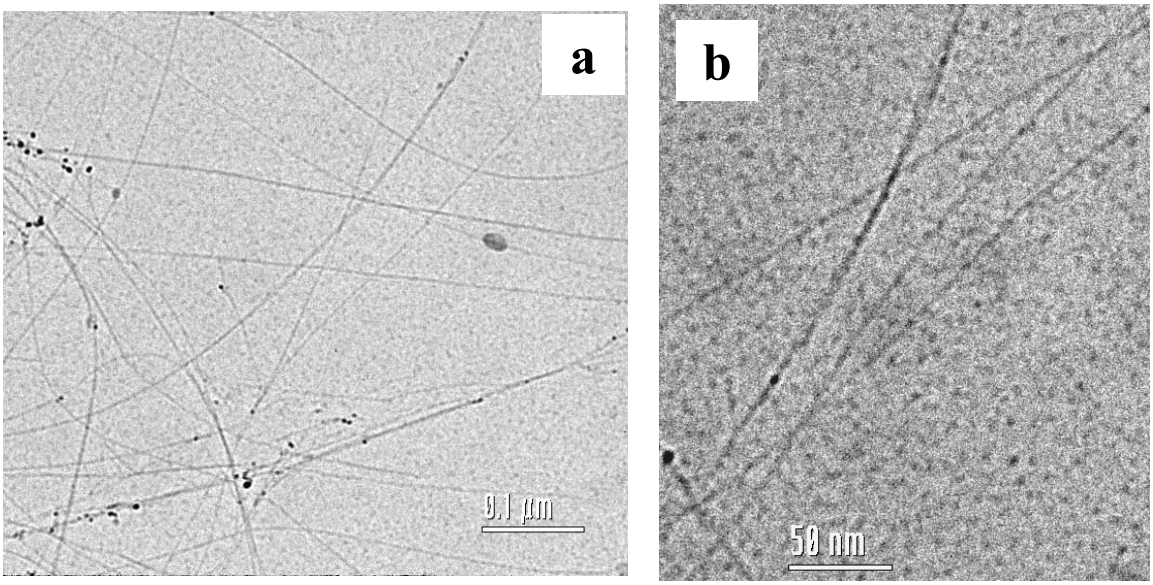


Figure 14: Cryo-TEM micrograph of SDS+PVP+ SWNT dispersion- Y.Talmon

**Electrospinning**

The electrospinning technique[28] was used to produce a composite nanofiber consisting of a continuous polymer matrix within which individual carbon nanotubes are embedded. Electrospinning was performed in the Department of Mechanical Engineering (Professors E. Zussman and A. Yarin) using an experimental apparatus as described elsewhere.[29] Arrays of oriented nanofibers were obtained, using electrospinning onto a vertical tapered rotating disk (diameter of *20 cm*). The jet flows downward from the surface of a pendant drop of fluid toward a rotating disc collector at a distance $h$ = 150 mm below the droplet. An electric field *15 kV / 20 cm* and an additional pressurization of the polymer solutions at the die by excess air pressure of *0.1-0.3 kg/cm*$^2$, were adjusted, to obtain a stable electrospinning process for all the tested solutions. The die diameter was *0.5 mm* (a syringe needle). The angular speed of the tapered disk was about *500 rpm*. The disc has a tapered edge in order to create a stronger converging electrostatic field.

Stable dispersions of multi-walled carbon nanotubes (MWNT, NanoLab Inc.) in SDS and in GA were mixed with aqueous solution of poly(ethylene oxide) [PEO, molecular weight~$10^6$, Aldrich] to form viscous spinnable composite solution according to the following table: Both dispersions of MWNT with GA and SDS (without PEO) were not spinnable and no nanofiber could be formed.

| No. | Carbon Namotubes Dispersion | PEO solution | Final composition |
|---|---|---|---|
| 1. | 0.37 % wt MWNT<br>1% wt GA | ~ 4 % wt<br>(MW=900000)<br>60:40 Ethanol:water | ~0.095 % wt MWNT<br>~0.25% GA<br>~0.3 % PEO |
| 2. | 0.7 % wt MWNT<br>2 % SDS | 6 % wt<br>(MW=600000)<br>60:40 Ethanol:water | ~0.35 % MWNT<br>~1 % SDS<br>~ 3 % PEO |

An X-ray diffraction photograph of PEO nanofiber, PEO+SDS nanofiber and PEO+SDS+MWNT nanofiber is given in **figure 15**. The diffraction pattern of PEO nanofiber (figure 15a) reveals high orientation of the PEO molecules along the fiber axis as indicated by the arcs in the equatorial reflection. The nanofibers composed PEO and SDS show even higher degree of orientation of the PEO crystals. Furthermore, the scattering from the SDS crystals at small angles (near the beam-stop) also exhibit a very high degree of orientation (figure 15b). The SDS chains are oriented perpendicular to the fiber axis. It sems that the orientation is significantly diminished when nanotubes are added to the spinning solutiun (figure 15c) These are only preliminary results and much is needed to be studied further.

Figure 15: X-ray diffraction of (a) PEO nanofiber
(b) PEO+SDS nanofiber
(c) PEO+SDS+MWNT nanofiber.

TEM micrographs of the "composite" nanofibers are presented in **figure 16**. The carbon nanotubes are clearly seen to be incorporated into the nanofibers as individual and not as bundles. In addition, a general alignment of the nanotubes along the nanofiber axis is achieved although waviness (figure 16b) and twisting of the nanotubes (figure 16a) are observed. These phenomena are probably related to electrospinning process.

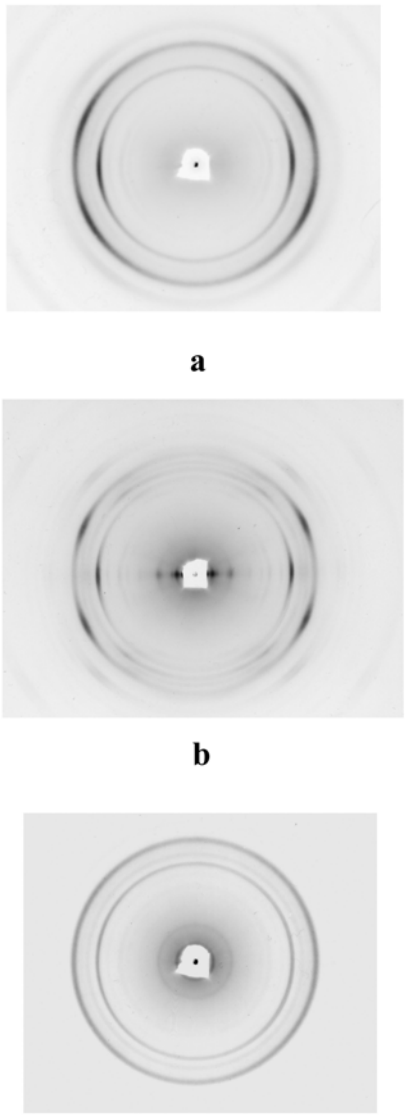


Figure 15:

X-ray diffraction of (a) PEO nanofiber (b) PEO+SDS nanofiber (c) PEO+SDS+MWNT nanofiber.

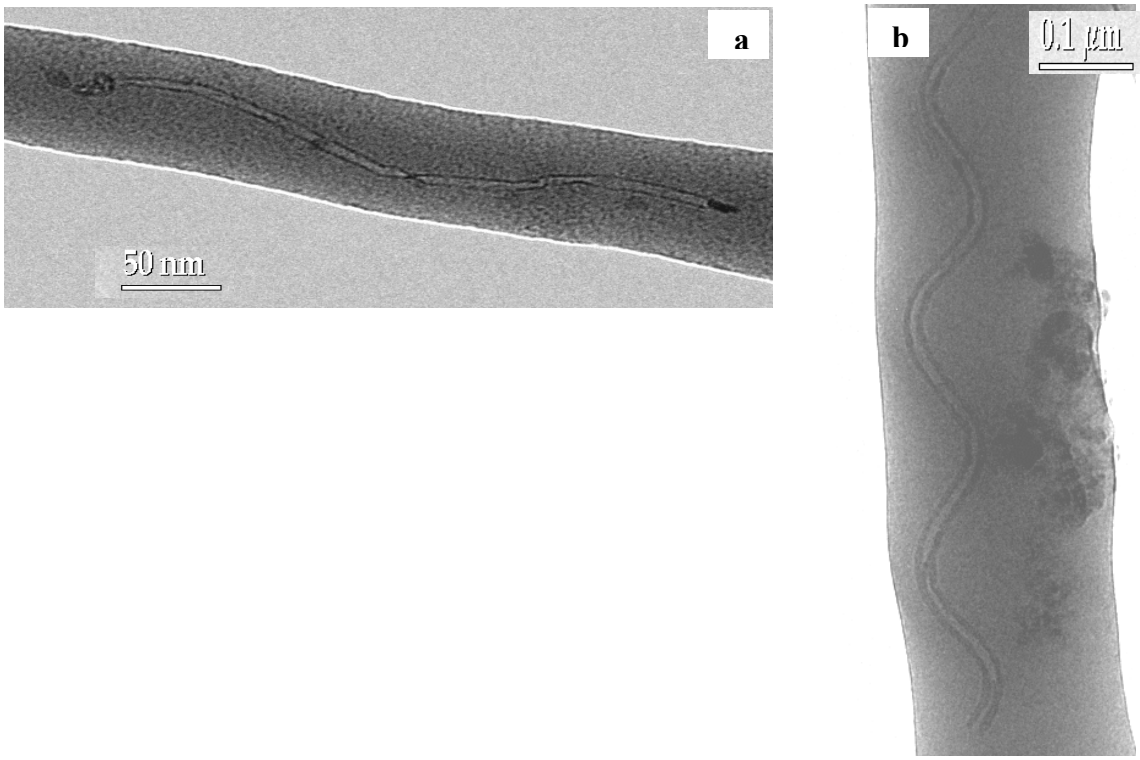


Figure 16: TEM micrographs of (a) SDS+PEO+MWNT nanofiber and (b) GA+PEO+MWNT nanofiber

## Conclusions

Stable dispersion of SWCNTs was achieved in the following amphiphilic polymers (in decreasing order of dispersing power) gum arabic, alternating copolymer of styrene and sodium maleate, polyvinyl pyrrolidone. The best dispersions were obtained with the natural polymer gum arabic. Studies on this polymer in aqueous solution indicate the origin of the dispersive interactions:

- a minority hydrophobic component can attach to the hydrophobic graphene layer.
- a highly branched, high molecular weight polymer structure with a hydrophilic nature forms a solvent-swollen protective layer due to entropic repulsion.
- charged groups at the ends of the polymer branches enhance swelling of the hydrophilic polymer layer and adds electrostatic repulsion.

Small angle neutron scattering measurements which were planned were not executed due to severe malfunction in the ISIS facility (UK).

The electrospinning process was successfully implemented using an electric field assisted take-up bobbin, by which oriented bundles of polymer-encapsulated. This was done using MWCNT dispersed in water/ethanol solutions containing poly(ethylene oxide) - PEO and surfactant (sodium dodecyl sulfate-SDS). TEM imaging displays individual tubes within PEO nanofibers, oriented along the fiber direction in some areas. Wide-angle x-ray diffraction indicated that the overall orientation achieved in the composite nanofibers was inferior to that of PEO alone. The highest orientation was achieved in PEO/SDS nanofibers, were the results indicate that both PEO crystals and SDS cylinders are oriented preferentially along the nanofiber axis.

## References


1) S.Iijima, *nature* **354**, 56 (1991).
2) T.W Ebbesen, *Acc Chem Res* **31**, 558 (1998).
3) M.S.Dresselhaus and M.Endo, *Applied Physics* **80**, 11 (2001).
4) P.M.Ajayan and O.Z.Zhou, *Topics Applied Physics* **80**, 391 (2001).
5) J.H.Hafner, C.L.Cheung, A.T.Wooley and C.M.Lieber, *Progress in Biophysics & Molecular Biology* **77**, 73 (2001).
6) P.Hadley and P.Heij, *unknown* (2002).
7) H.M.Cheng, Q.H.Yang and C.Liu, *Carbon* **39**, 1447 (2001).
8) M.S.P.Shaffer, X.Fan and A.H.Windle, *Carbon* **36**, 1603 (1998).
9) K.Esumi, M.Ishigami, A.Nakajima, K.Sawada and H.Honda, *Carbon* **34**, 279 (1996).
10) J.Chen, M.A.Hamon, H.Hu, Y.Chen, A.M.Rao, P.C.Eklund and R.C.Haddon, *Science* **282**, 95 (1998).
11) E.T.Mickelson, C.B.Huffman, A.G.Rinzler, R.E.Smalley, R.H.Hauge and J.L.Margrave, *Chemical Physics Letters* **296**, 188 (1998).
12) M.Monthioux, B.W.Smith, B.Burteaux, A.Claye, J.E.Fischer and D.E.Luzzi, *Carbon* **39**, 1251 (2001).
13) I.W.Chiang, B.E.Brinson, A.Y.Huang, P.A.Willis, M.J.Bronikowski, J.L.Margrave, R.E.Smalley and R.H.Hauge, *J.Phys.Chem.B* **105**, 8297 (2001).
14) B.Vigolo, A.Penicaud, C.Coulon, C.Sauder, R.Pailler, C.Journet, P.Bernier and P.Poulin, *Science* **290**, 1331 (2000).
15 A.B.Dalton, C.Stephan, j.N.Coleman, B.McCarthy, P.M.Ajayan, S.Lefrant, P.Bernier, W.J.Blau and H.J.Byrne, *J.Phys.Chem.B* **104**, 10012 (2000).
16) J.N.Coleman, A.B.Dalton, S.A.Curran, A.Rubio, P.Davey, A.Drury, B.McCarthy, B.Lahr, P.M.Ajayan, S.Roth, R.C.Barklie and W.J.Blau, *Advanced Materials* **12**, 213 (2000).
17) S.A.Curran, P.M .Ajayan, W.J.Blau, D.L.Carroll, j.N.Coleman, A.B.Dalton, A.P.Davey, A.Drury, B.McCarthy, S.Maier and A.Strevens, *Advanced Materials* **10**, 1091 (1998).
18) B.McCarthy, S.A.Curran, A.B.Dalton, A.P.Davey, Z.Konya, A.Fonseca, J.B.Nagy and W.J.Blau, *J.Materials Sceince Letters* **19**, 2239 (2000).

19) A.B.Dalton, W.J .Blau, G.Chambers, j.N.Coleman, K.Henderson, S.Lefrant, B.McCarthy, C.Stephan and H.J.Byrne, *Synthetic Metals* **121**, 1217 (2001).

20) M.J.O'Connell, P.J.Boul, L.M.Ericson, C.B.Huffman, Y.Wang, E.Haroz, C.Kuper, J.Tour, K.D.Ausman and R.E.Smalley, *Chemical Physics Letters* **342**, 265 (2001).

21) R.Bandyopadhyaya, E.Nativ-Roth, O.Regev and R.Yerushalmi-Rozen, *Nano Letters* **2**, 25 (2002).

22) P.Launois, A.Marucci, B.Vigolo, P.Bernier, A.Derre and P.Poulin, *J.Nanosicence and Nanothecnology* **1**, 125 (2001).

23) H.Schreuder-Gibson, K.Senecal, M.Sennett and L.Samuelson, *Proc.Electrochem.Soc.* 2000 (2000).

24) S.Kumar, X.Zhang, A.R.Bhattacharyya, B.G.Min, T.D.Dang, F.E.Arnold, R.A.Vaia, S.Ramesh, P.A.Willis, R.H.Hauge, and R.E.Smalley. Structure and properties of poly(para phenylene benzobisoxazole) (PBO) /single wall carbon nanotube composite fibers. American Phys.Soc, Meeting . 2002.

25) I.W.Chiang, B.E.Brinson, A.Y.Huang, P.A.Willis, M.J.Bronikowski, J.L.Margrave, R.E.Smalley and R.H.Hauge, *J.Phys.Chem.B* **105**, 8297 (2001).

26) Talmon, Y. In *Modern Characterization Methods of Surfactant Systems*; Binks, B. P., Ed.; Marcel Dekker: New York, 1999; pp 147-178.

27) S.Rols, E.Anglaret, J.L.Sauvajol and A.J.Dianoux, *Applied physics A* **69**, 591 (1999).

28) D.H.Reneker, A.L.Yarin and H.F.and S.Koombhongse, *J.Appl.Phys.* **87**, 4531 (2000).

29) A.Theron, E.Zussman and A.L.Yarin, *Nanotechnology* **12**, 384 (2001).

## APPENDIX

Y. TSABBA, D.M. REIN, Y. COHEN,

"Effect of Coagulation Conditions on the Microfibrillar Network of a Rigid Polymer"

Journal of Polymer Science: PartB: Polymer Physics,Vol.**40**, 1087–1094 (2002)

# Effect of Coagulation Conditions on the Microfibrillar Network of a Rigid Polymer

**YIZHAK TSABBA, DMITRY M. REIN, YACHIN COHEN**

Department of Chemical Engineering, Technion-Israel Institute of Technology, Technion City, Haifa 32000, Israel

*Received 24 September 2001; revised 1 March 2002; accepted 4 March 2002*

**ABSTRACT:** An important element in the microstructure of high performance fibers and films fabricated from rigid polymers is an interconnected network of oriented microfibrils, the lateral size of which is about 10 nm. This study is an attempt to elucidate the mechanism by which the microfibrils are formed so that larger lateral dimensions can be achieved by suitable processing. Because this morphology emerges in the coagulation stage of the spinning process, we compared the microfibrillar network formed by drastically different coagulation conditions. Ribbons, spun from solution of poly(*p*-phenylene benzobisthiazole) in polyphosphoric acid through a slit die, were coagulated either in the ordinary rapid process with water (timescale of seconds) or in a slow process with phosphoric acid (timescale of hours). The coagulated microfibrillar network was dried with supercritical $CO_2$ for X-ray scattering measurements and impregnated with epoxy resin for sectioning and imaging by TEM. Slow coagulation yields better-aligned microfibrils of enhanced chain packing, but the lateral size of the microfibrils formed in both cases is similar, about 10 nm. Heat treatment increases the width of water-coagulated microfibrils but not the acid-coagulated ones. The observations do not support spinodal decomposition as the mechanism of microfibril formation during coagulation, as was previously suggested. © 2002 Wiley Periodicals, Inc. J Polym Sci Part B: Polym Phys 40: 1087–1094, 2002

**Keywords:** high performance polymers; poly(*p*-phenylene benzobisthiazole); microstructure; SAXS; TEM

## INTRODUCTION

Polymer fibers of exceptionally high tensile properties can be attained when the polymer chain is fully extended. This may be achieved by synthesis of rigid-chain polymers, such as the aromatic heterocyclic rigid-chain polymers, developed by the U.S. Air Force Ordered Polymers Program.[1] These rigid polymers are, however, processable only from solutions in strongly interacting solvents, such as strong acids. Two examples from this group of rigid polymers are *trans*-poly(*p*-phenylene benzobisthiazole) (PBZT) and *cis*-poly(*p*-phenylene benzobisoxazole) (PBZO). The processing, properties, and structure of PBZT have been studied extensively during the last two decades.[1] PBZO has been commercialized as Zylon,™ and studies relating its morphology and properties have been reported.[2–4] Fibers are processed from solutions in polyphosphoric acid (PPA), which is their polymerization medium.[5] In the spinning process, a liquid-crystalline solution is extruded through a spinneret into a coagulation bath containing a nonsolvent that is usually water. Extensional flow in a narrow air gap separating the spinneret and the coagulation bath results in a high degree of chain orientation. The solution stream solidifies in the coagulation bath by trans-

*Correspondence to:* Yachin Cohen (E-mail: yachinc@tx.technion.ac.il)

Journal of Polymer Science: Part B: Polymer Physics, Vol. 40, 1087–1094 (2002)
© 2002 Wiley Periodicals, Inc.

formation from an oriented liquid-crystal state to a crystalline solid state. The microstructure formed in the coagulation stage of PBZT fiber spinning was an interconnected network of oriented microfibrils, the width of which is of the order of 10 nm, and with a void content exceeding 80%.[6,7] The void-space is collapsed during drying to an order of 1%. Subsequent heat treatment enhances the degree of orientation, perfection of crystalline packing, and overall mechanical properties of the fiber.[8] The lateral width of the polymer crystals does not increase beyond the limit set by the lateral dimensions of the microfibrils formed during coagulation. Heat treatment does not seem to increase significantly the dimensions of the microfibrils.[9] This limitation on the lateral crystal size, resulting from the limit of the microfibril dimension set by the coagulation process, is considered to be an impediment for achieving enhanced properties, particularly compressive strength. It was postulated that collective buckling of the microfibrils is the cause of kink-band formation that leads to ultimate failure.[6]

The changes that occur during coagulation in the fiber-spinning process, where the microfibrillar morphology is set, are complex. The oriented liquid-crystalline solution of the protonated rigid polymer in its acid solvent is transformed to the crystalline state, following deprotonation of the polymer by the coagulant. The ternary phase diagram of a rigid polymer (PBZT), acid solvent, and coagulant (water) has been analyzed in detail.[10] Although the reported study[10] was performed using low molecular weight (MW) PBZT in methane-sulfonic acid, its qualitative features are relevant to the higher MW PBZT/PPA system. Two intermediate crystalline forms, termed *crystal-solvate phases*, exist between the liquid (isotropic or liquid crystalline) and the crystalline polymer state. The form-I crystal solvate, identified as a cocrystal of the protonated polymer and the solvent anions, was observed in PPA solutions of PBZT[11] and PBZO.[12] The form-I crystals that occur by absorption of very small amounts of moisture into a polymer-acid solution can exhibit large-scale structures such as spherulites of extended-chain lamellae.[10] These exhibit a rather low melting/dissolution temperature, below 100 °C.[12,13] The form-II crystal solvate, considered a polymer-solvent cocrystal in which the polymer is deprotonated,[11,12] exhibits a higher melting point, about 300 °C.[12] Pure polymer crystals do not exhibit a melting point below the decomposition temperature. The coagulation transformation in a typical spinning process, when water is used as the coagulant, occurs rapidly. Studies on equilibrium crystal-solvate phases have suggested that a slow coagulation process in which crystal-solvate phases are initially formed may affect the microfibrillar morphology.

Past efforts to explain the formation mechanism of the microfibrillar morphology invoked a diffusion-limited crystallization process[14] as well as anisotropic spinodal decomposition.[15,16] There is no model that can predict the way in which the coagulation process controls the microfibrillar dimensions or whether the limiting lateral size of about 10 nm can be surpassed. An undisclosed change in the coagulation conditions of Zylon™ fibers, by use of a nonaqueous slow coagulant, was reported to result in an enhanced tensile modulus. This was related to an enhanced degree of orientation and near-elimination of disordered regions in the crystalline packing. The presence of such disordered regions in water-coagulated fibers has been reported to yield a four-point small-angle X-ray scattering (SAXS) pattern.[17,18] Alternatively, the four-point pattern was explained by the shape factor of crystalline grains, particularly because of (302) grain boundaries.[19] In any case, an enhanced modulus was attributed to a more homogeneous structure with less defect regions having a concentration of chain ends that can reduce the overall modulus.[20] Whatever the origin of microstructural inhomogeneities resulting in the four-point SAXS pattern, their lateral dimensions do not exceed about 10 nm, the lateral size of the microfibrils formed during coagulation. Furthermore, the lateral dimensions of the crystals in the highest modulus fiber, obtained after heat treatment of the slow-coagulated fiber, still do not exceed the 10-nm limit.[3]

The objective of this study is to evaluate the effect of a controlled slow-coagulation process on the microfibrillar morphology of rigid polymer fibers. The typical aqueous process is compared with coagulation in 85% phosphoric acid. This coagulant can be considered as part of the PPA water system, without incorporating additional chemical species.

## EXPERIMENTAL

### Sample Preparation

PBZT dope in PPA, containing 15% PBZT (intrinsic viscosity of 26 dL/g in methane sulfonic acid,

MW ~ 41 kDa) in PPA (82.6% $P_2O_5$) was obtained from the Polymer Branch, Materials and Manufacturing Directorate, U.S. Air-Force Research Laboratory. Ribbons were spun through a slit die and extended (three times) in air. The extrudate was coagulated either in water or 85% phosphoric acid. In both cases, the ribbons were kept in the coagulation medium. The phosphoric acid was diluted gradually over a period of 14 days, and the ribbons were subsequently washed in water. To minimize collapse of the microfibrillar network that would occur by conventional drying, a critical-point drying procedure was used, as reported previously.[9] The ribbons imbibed with water were first gradually dehydrated with acetone over a period of 2 days. The samples were then washed with liquid $CO_2$ in a Polaron critical-point drier and subsequently dried by raising the temperature beyond the critical point of $CO_2$. To study the effect of heat treatment, critical-point dried films were heat treated in a vertical tube furnace at 450 °C and 0.5 MPa tension under nitrogen for 10 min.

### X-ray Scattering Measurements

SAXS measurements and the method of data analysis have been reported.[9] In brief, a slit-collimated Kratky compact camera (A. Paar Co.) was used with Ni-filtered Cu K$\alpha$ radiation (sealed-tube generator at 40 kV and 30 mA). The spun ribbon was placed with the spinning direction parallel to the slit-length direction of the incident beam. Scattering in the perpendicular plane was measured with a linear position-sensitive detector (Raytech) coupled to a multichannel analyzer. The sample to detector distance was 260 mm. The increment of scattering vector per channel was 0.0126 $nm^{-1}$. The scattering vector is defined as $h = 4\pi \sin\theta/\lambda$ (where $2\theta$ is the scattering angle, and $\lambda$ is the wavelength).

Wide-angle diffraction patterns in the equatorial direction, perpendicular to the spinning direction, were measured using a Siemens powder diffractometer. The sample was placed with its chain axis parallel to the length of the incident beam and to the rotation axis of the goniometer.

### Transmission Electron Microscopy (TEM)

Samples of PBZT ribbons were impregnated with epoxy resin, as described previously.[6] Longitudinal and transverse sections were obtained with a Reichert FC-4D ultramicrotome using a Diatome diamond knife. The sections were imaged in a JEOL JEM-2000FX TEM operated at 100 KV using a 30 $\mu$m objective aperture. Electron diffraction was measured using a small selected area diffraction aperture (25 $\mu$m) for which the virtual aperture is about 1 $\mu$m.

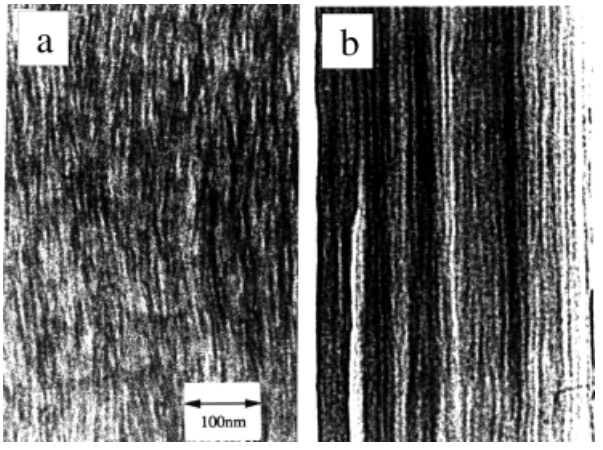


**Figure 1.** TEMs of longitudinal sections of PBZT ribbons coagulated in water (a) and in phosphoric acid (b) after critical-point drying and impregnation with epoxy resin. The spinning and cutting directions are vertical.

## RESULTS AND DISCUSSION

This study was motivated by the quest to control the lateral size of microfibrils in rigid-polymer fibers that are formed in the coagulation stage of the spinning process. The conjecture was that a much slower transformation may yield larger and more perfect solid structures. The rate of transformation from solution to the solid state was controlled by the coagulation medium. Using water, the crystalline PBZT phase emerges within a few seconds, as noted by a color change from dark green to yellow-orange.[11] On the other hand, it takes about 5 h for the color of the PBZT ribbon to change to dark red when it is coagulated in phosphoric acid.[11] The red state was determined to be the form-II PBZT/PPA crystal solvate, which only upon subsequent washing with water transforms to the crystalline PBZT state.[10,11]

TEM images of longitudinal sections of water-coagulated and acid-coagulated PBZT ribbons, after super-critical-point drying, are shown in Figures 1(a,b), respectively. The long dark striations oriented along the extrusion direction are the microfibrils embedded in the epoxy matrix. Their dark appearance is due to both diffraction and

mass contrast. Two observations are directly evident. The microfibrils formed by acid coagulation appear much better oriented than the water-coagulated ones, but the lateral size of the microfibrils appears to be similar, about 10 nm. Although similar in lateral size, the microfibrils formed by acid coagulation appear to proceed in a straight manner throughout the image, whereas the water-coagulated ones appear to be more contorted and have more junctions along their length.

The similarity in lateral size of the water- and acid-coagulated microfibrils is verified by analysis of the SAXS patterns, presented in Figure 2. In this experiment, the scattering from a highly oriented sample with fiber symmetry is measured with a slit-collimated incident beam oriented parallel to the fiber axis and a linear detector perpendicular to it. This measurement yields information about the structure in a cross-section plane perpendicular to the fiber axis.[21] The lateral size of the microfibrils can be calculated from scattering laws derived for a two-phase structure with sharp interfaces,[22] which is a very reasonable assumption in this case. If the average microfibrillar cross section is approximated as a circle having the same average circumference length per unit area, then this diameter $\bar{D}$ can be measured by[7,9]

$$\bar{D} = \frac{\langle D^2 \rangle}{\langle D \rangle} = \frac{4Q}{\pi(1 - v_f)K_p} \tag{1}$$

where $Q$ is given by

$$Q = \int_o^{\mathbf{h}\,\max} [I(h) - F]hdh + \frac{K_p}{h_{\max}} \tag{2}$$

where $h_{\max}$ is the value of the largest scattering vector in the measured data, and $K_p$ and $F$ are obtained from a Porod law fit to the data, which in the cross-section plane is[22]

$$I(h) = \frac{K_p}{h^3} + F \tag{3}$$

The volume fraction of microfibrils $v_f$ (assumed equal to their areal fraction in a cross-section plane) was evaluated from measurements of X-ray absorption and sample thickness, as in previous studies.[7,9] The apparent average microfibril diameters, thus calculated for the water- and acid-coagulated PBZT ribbons before and after heat treatment, are summarized in Table 1. The scattering patterns from the critical-point dried

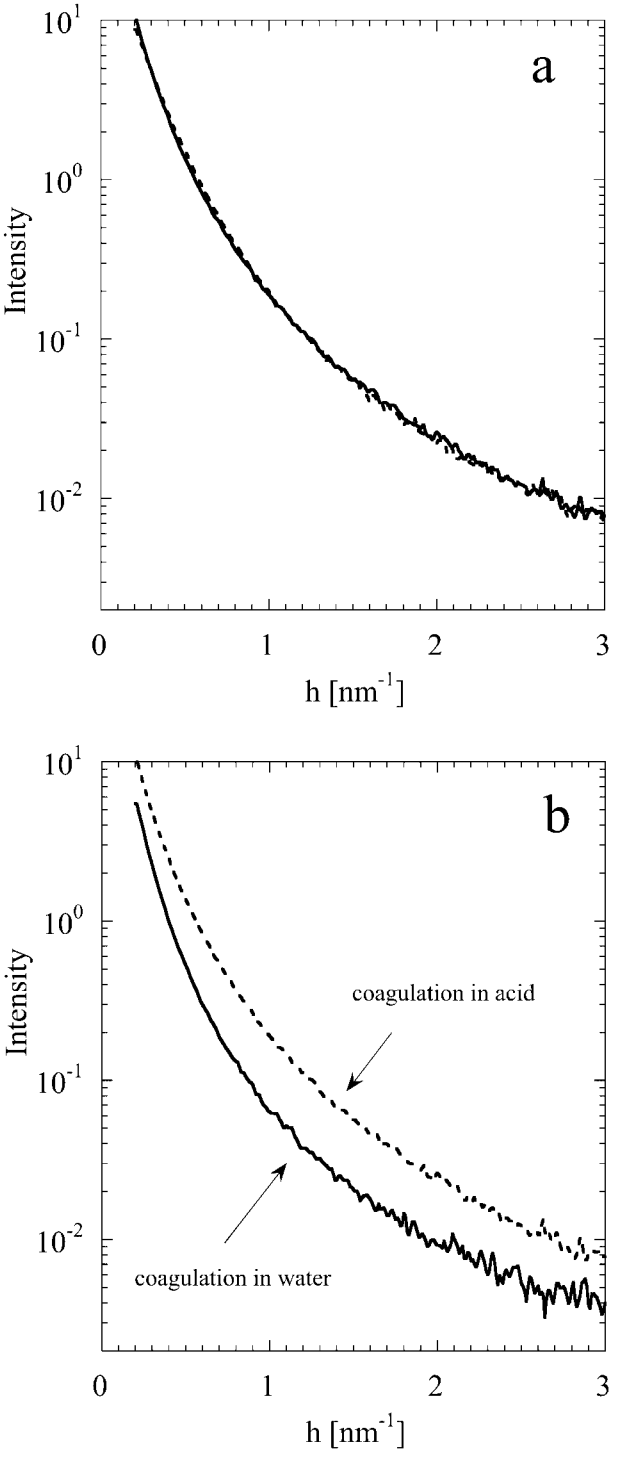


**Figure 2.** SAXS patterns from PBZT ribbons coagulated in water (solid line) and phosphoric acid (dashed line) after critical-point drying (a) and heat treatment (b).

**Table 1.** Microfibril Characteristics as a Function of Processing Conditions Measured by SAXS

| Processing Conditions | Microfibril Volume Fraction $v_f$ | Apparent Lateral Size $\bar{D}$ (nm) |
|---|---|---|
| Water-coagulated (wc) | 0.37 | 11 |
| Acid-coagulated (ac) | 0.34 | 11 |
| wc after heat treatment | 0.53 | 20 |
| ac after heat treatment | 0.40 | 15 |

PBZT ribbons obtained either by a typical rapid coagulation in water or by the very slow coagulation process in phosphoric acid are nearly identical, as shown in Figure 2(a). They yielded a value for the apparent microfibril diameter of 11 nm in both cases. This proves clearly that the significant slowing-down of the coagulation process has no effect on the lateral dimension of the emerging microfibrils. However, acid coagulation results in better-aligned microfibrils, as indicated in Figure 1. Moreover, the degree of crystalline order in the lateral packing of PBZT chains within the microfibrils is also enhanced by acid coagulation. Figure 3 describes wide-angle X-ray diffraction patterns in the equatorial plane from water- and acid-coagulated PBZT ribbons after critical-point drying. The observed reflections are broad, and it is difficult to evaluate accurately the apparent crystal size from the peak breadths. The pattern from the acid-coagulated sample exhibits sharper reflections that follow the known unit cell of PBZT,[23] and the peaks at about 25 and 50° begin to exhibit resolution of the individual reflections. A rudimentary analysis indicates that the apparent crystal size is smaller than the lateral size of the microfibrils but that acid-coagulation results in somewhat larger crystals.

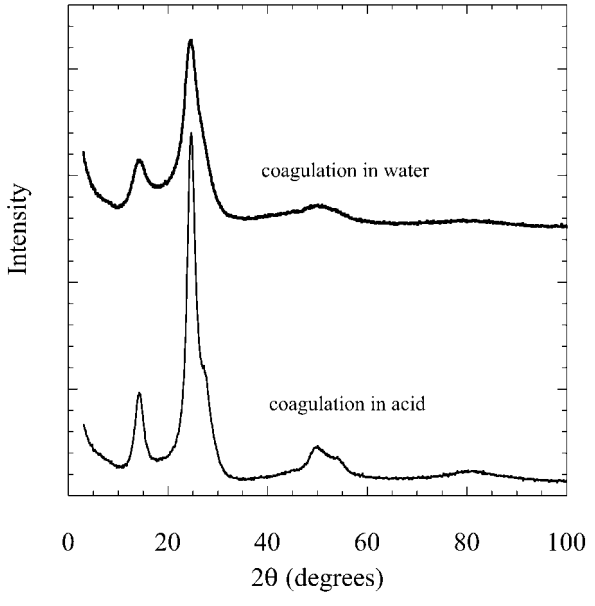


**Figure 3.** Diffractometer scans of the equatorial reflections from the critical-point dried PBZT ribbons. Top: coagulated in water; bottom: coagulated in acid.

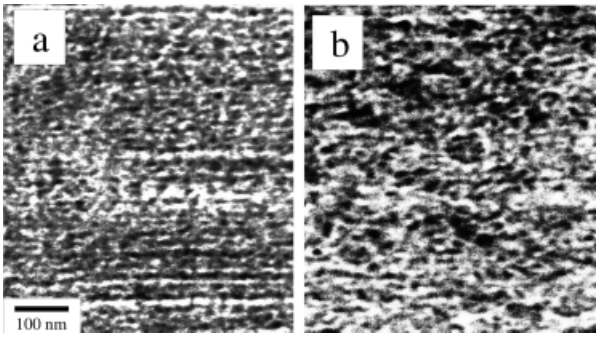


**Figure 4.** TEMs of transverse sections of PBZT ribbons coagulated in phosphoric acid before (a) and after heat treatment (b).

The effect of heat treatment on water-coagulated PBZT microfibrils has been reported.[9] An increase of about 50% in the apparent lateral size was observed. The fact that acid coagulation resulted in better-aligned microfibrils, as shown in the TEM images in Figure 1, suggests that their behavior under heat treatment may be different. The heat treatment used in this study (10 min at 450 °C) differs from the previous study (10 s at 600 °C). The scattering patterns from the heat-treated ribbons are depicted in Figure 2(b), and the characteristics evaluated by their analysis are given in Table 1. In the case of water-coagulated ribbons, heat treatment resulted in a significant increase of the lateral size, whereas the acid-coagulated ones showed a smaller effect. The effect of heat treatment on the microfibrillar structure can also be evaluated by TEM images of thin samples sectioned perpendicular to the spinning direction. Figures 4(a,b) indicate cross sections of an acid-coagulated ribbon before and after heat treatment, respectively. The cross sections of the microfibrils appear as irregularly shaped objects, the lateral dimension of which seems to increase with heat treatment as measured by SAXS. The slight striations appearing in the horizontal direction are artifacts of cutting. Electron diffrac-

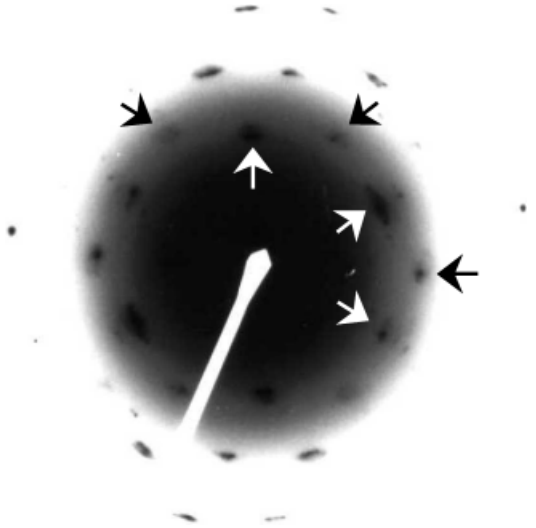

**Figure 5.** Electron-diffraction pattern from a transverse section of a PBZT ribbon after critical-point drying and heat treatment. White arrows point to (010) reflections at a spacing of about 0.354 nm, and dark arrows point to (400) reflections at 0.295 nm spacing, with the reciprocal unit-cell angle $\gamma^*$ at about 86°.

tion from the cross sections usually appeared as homogeneous rings, indicating uniaxial symmetry about the spinning direction. However, electron-diffraction patterns from cross sections of water-coagulated samples after heat treatment appeared spottier and in some cases could be resolved to individual single-crystal-like patterns. An example is illustrated in Figure 5. The polycrystalline texture seems to be organized about three main orientations, each rotated by about 60–65°. In Figure 5, white arrows point to (010) reflections at a spacing of about 0.354 nm, and dark arrows point to (400) reflections at 0.295 nm spacing, with the reciprocal unit-cell angle $\gamma^*$ about 86°. This indicates that in regions giving rise to such a pattern there exists a large degree of coherence in the spacing of PBZT chains in regions that encompass many microfibrillar cross sections. An enlarged view of a cross section in the water-coagulated ribbon after heat-treatment, shown in Figure 6, indicates that the microfibril cross section assumes in several cases a lozenge shape and that several microfibrils seem to be clustered together. It is not clear why water-coagulated microfibrils exhibit larger growth in lateral size during heat treatment as compared with the acid-coagulated ones and even show coherently packed chains encompassing many neighboring microfibrils. This may be related to the fact that the microfibrils in the water-coagulated ribbons have an initial morphology that is rather contorted with more junctions and other imperfections. Although this fact most likely results in more defects along the microfibril axis, it may provide more flexibility for adjacent microfibrils, particularly near junction regions, to coalesce.

The conjecture of this study was that the coagulation rate affects the microfibrillar morphology by controlling the transformation kinetics. This reasoning followed from considerations of the following two main mechanisms proposed for the transformation from the oriented nematic solution to the microfibrillar network: crystallization or spinodal decomposition. It is often observed that the depth of quench from the equilibrium phase boundary controls both the rate of the transformation as well as the dimensions of the emerging structures. Rapid transformations are most often associated with smaller structures. The apparent insensitivity of the microfibrillar thickness to the coagulation conditions suggests that the transformation mechanism is not spinodal decomposition. By the basic view of spinodal decomposition,[24] the rate of material transport is proportional to $-(\partial^2 G/\partial c^2)_{T,P}$ (where $G$ is the free-energy density, and $c$ is concentration), whereas the characteristic size of the fastest growing fluctuation is inversely related to it. Thus, spinodal decomposition that occurs at a low

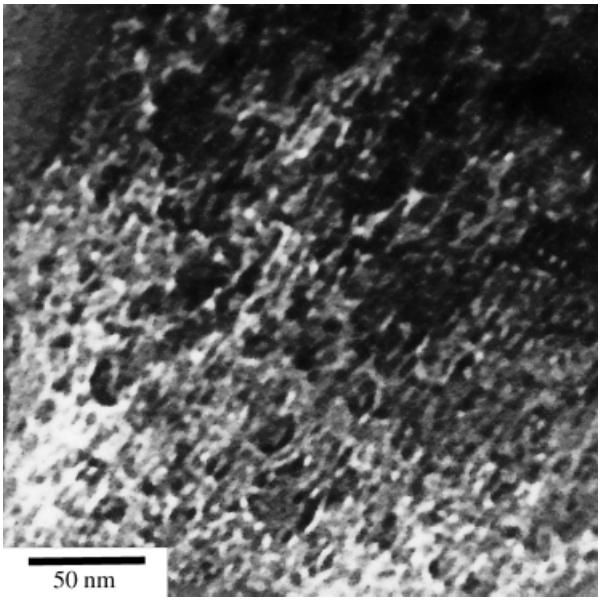


**Figure 6.** Enlarged image by TEM of a transverse section of a PBZT ribbon coagulated in water and heat treated at 450 °C for 10 min.

quench into the biphasic region, where the convexity of the free-energy curves is small, is expected to yield slowly evolving structures of relatively large dimensions, as compared with rapid evolution of smaller structures in a deeper quench. We consider water coagulation as a deep quench into the biphasic region of the rigid-polymer/solvent/nonsolvent phase diagram[10] and coagulation with phosphoric acid as a shallow quench. Thus, the observation that the drastic slowing down of the transformation by acid coagulation is not accompanied by larger structures in the transformed microfibrillar state is against spinodal decomposition as the transformation mechanism. If we consider nucleation and growth of PBZT crystalline phases as the transformation mechanism, a similar argument would hold against a nucleation-controlled process. The observations of this study can be reconciled with a diffusion-controlled, crystallization process. As a possible source of crystal nuclei, we may consider the form-I crystal solvates that occur at a very low amount of coagulant and that may precede the transformation to the microfibrillar PBZT crystal or form-II crystal-solvate state.

Considering the transformation mechanism, it is also necessary to consider issues of molecular mobility, both of the coagulant and the crystallizing polymer. Coagulant molecules need to diffuse from the coagulation medium into the PBZT solution. The higher viscosity of phosphoric acid as compared with water indicates a lower mobility. Water diffusion is further enhanced by a larger difference in the chemical potential because of more favorable water/PPA interactions. However, the main difference between the two types of coagulant is in the crystal solvate form that first evolves. In the case of water, it is the form-II crystal solvate in which PBZT chains are deprotonated, whereas in the case of acid coagulation it is the form-I crystal solvate that is a cocrystal of protonated PBZT and PPA anions. As previously mentioned, the fact that these two extreme cases result in similar microfibril dimensions despite a large perceived difference in the thermodynamic undercooling indicates that structure formation is controlled by polymer diffusion. The length of the rigid PBZT chain (estimated ca. 200 nm) is much larger then the lateral size of the microfibrils and the spacing between them. Thus, only a rather limited lateral motion is required to form the crystalline aggregates that are the basis for the microfibrils.

## CONCLUSION

Ribbons of an oriented PBZT solution in PPA were coagulated in two drastically different processes—rapid coagulation in water (timescale of seconds) or slow coagulation in 85% phosphoric acid (timescale of hours). Slow coagulation yields better-aligned microfibrils of enhanced chain packing, but the lateral size of the microfibrils formed in both cases is similar, about 10 nm. Heat treatment increases the width of water-coagulated microfibrils much more then the acid-coagulated ones. The observations do not support spinodal decomposition as the mechanism of microfibril formation during coagulation, as was previously suggested. However, this mechanistic conclusion is far from being definitive. The origin and control of the microfibrillar size in rigid-polymer fibers remain open questions that require further study. This study has shown that slow coagulation yields better-aligned microfibrils of enhanced chain packing that may be the source of an enhanced tensile modulus observed recently.[3]

The authors gratefully acknowledge financial support by the U.S. Air Force - European Office of Aerospace Research and Development. The authors also thank Dr. R. Evers of the Polymer Branch, Materials and Manufacturing Directorate at the Air Force Research Laboratory for the gift of PBZT as well as Dr. W. W. Adams and Dr. R. Pachter for the helpful discussions. D. M. Rein's work was supported in part by a joint grant from the Center for Absorption in Science of the Ministry of Immigrant Absorption and the Committee for Planning and Budgeting of the Council for Higher Education under the framework of the KAMEA program.

## REFERENCES AND NOTES

1. See for example The Materials Science and Engineering of Rigid-Rod Polymers. In Materials Research Society Symposium Proceedings; Adams, W. W.; Eby, R. K.; McLemore, D. E., Eds.; 1989; Chapters 5 (Properties) and 6 (Morphoplogy) p 134.
2. Kitagawa, T.; Murase, H.; Yabuki, K. J Polym Sci Part B: Polym Phys 1998, 36, 39–48.
3. Kitagawa, T.; Ishitobi, M.; Yabuki, K. J Polym Sci Part B: Polym Phys 2000, 38, 1605–1611.
4. Kitagawa, T.; Yabuki, K. J Polym Sci Part B: Polym Phys 2000, 38, 2901–2911.
5. Wolfe, J. F.; Loo, B. M.; Arnold, F. E. Macromolecules 1981, 14, 915–920.
6. Cohen, Y.; Thomas, E. L. Macromolecules 1988, 21, 433–436.

7. Cohen, Y.; Thomas, E. L. Macromolecules 1988, 21, 437–441.
8. Allen, S. R.; Farris, R. J.; Thomas, E. L. J Mater Sci 1985, 20, 4583–4592.
9. Cohen, Y.; Gartstein, E.; Arndt, K. F.; Ruland, W. Polym Eng Sci 1995, 36, 1355–1359.
10. Cohen, Y.; Cohen, E. Macromolecules 1995, 28, 3631–3636.
11. Cohen, Y.; Saruyama, Y.; Thomas, E. L. Macromolecules 1991, 24, 1161–1167.
12. Cohen, Y.; Adams, W. W. Polymer 1996, 37, 2767–2774.
13. Cohen, Y.; Buchner, S.; Zachmann, H. G.; Davidov, D. Polymer 1992, 33, 3811–3817.
14. Cohen, Y.; Thomas, E. L. Polym Eng Sci 1985, 25, 1093–1096.
15. Wang, W.; Ruland, W.; Cohen, Y. Acta Polym 1993, 44, 273–278.
16. Beltsios, K. G.; Carr, S. H. J Macromol Sci Phys 1990, 29, 71–89.
17. Bai, S. J.; Price, G. E. Polymer 1992, 33, 2136–2142.
18. Kumar, S.; Warner, S.; Grubb, D. T.; Adams, W. W. Polymer 1994, 35, 5408–5412.
19. Martin, D. C.; Thomas, E. L. Macromolecules 1991, 24, 2450–2460.
20. Jones, M. C. G.; Martin, D. C. Macromolecules 1995, 28, 6161–6174.
21. Perret, A.; Ruland, W. J Appl Cryst 1969, 2, 209–218.
22. Ruland, W. J Appl Cryst 1971, 4, 70–73.
23. Fratini, A. V.; Galen, P. G.; Resch, T. J.; Adams, W. W. The Materials Science and Engineering of Rigid-Rod Polymers. In Materials Research Society Symposium Proceedings; Adams, W. W.; Eby, R. K.; McLemore, D. E., Eds.; 1989; Chapters 5 (Properties) and 6 (Morphoplogy), p 431.
24. Cahn, J. W.; Hilliard, J. E. J Chem Phys 1958, 28, 257.